Investigation of the mechanical properties of mammalian cells through dielectrophoresis

vorgelegt von
Diplom-Ingenieurin
Isabella Guido
aus Carmiano (Italien)

Von der Fakultät V - Verkehrs- und Maschinensysteme
der Technischen Universität Berlin
zur Erlangung des akademischen Grades
Doktor der Ingenieurwissenschaften
Dr.-Ing.

genehmigte Dissertation

Promotionsausschuss:

Vorsitzender:	Prof. Dr.-Ing. Marc Kraft
Berichter:	Prof. Dr.-Ing. Christian Oliver Paschereit
Berichter:	Priv. Doz. Dr. rer. nat. Claus Duschl

Tag der wissenschaftlichen Aussprache: 27. Januar 2010

Berlin 2010

D 83

Ich habe keine besondere Begabung,
sondern bin nur leidenschaftlich neugierig.
(Albert Einstein)

Danksagung

Ich möchte mich gerne bei allen bedanken, die mich während meiner Promotion im Fraunhofer Institut für Biomedizinische Technik in Potsdam-Golm unterstützt haben.
Mein erster Dank richtet sich an meinen Arbeitsgruppenleiter Dr. Magnus Jäger für die exzellente Betreuung meiner Arbeit und für sein Vertrauen. In jeder Situation war er immer bereit für neue Vorschläge und für kompetente Diskussionen über die Vorstellung, die ich von meiner Arbeit hatte. Durch seine fachliche und persönliche Unterstützung habe ich es geschafft schwierige Momente meiner Arbeit durchzuhalten und die Motivation nicht zu verlieren.
Herrn Dr. Claus Duschl danke ich für seine hervorragende Betreuung, sowie für die Möglichkeit in seiner Abteilung zu promovieren. Seine fachliche Kompetenz, die er durch konstruktive Anregungen, Rat und Engagement mit mir geteilt hat, war immer sehr hilfreich und von großem Wert. Er schuf ein Arbeitsumfeld, das viel Freiraum zum Experimentieren ließ und die Diskussion unter den Mitarbeitern förderte.
Ich möchte mich bei Herrn Prof. Paschereit für seine unkomplizierte offene Betreuung und für die Freiheit der Auswahl meines Promotionsthemas bedanken.
Ein extra großes Dankeschön richte ich an Beate Morgenstern, die mir mit ihrer Erfahrung und Kompetenz die Zellkultivierung beigebracht hat. Ich möchte ihr besonders danken für ihre verständnisvollen und liebevollen Gespräche, sowohl fachlich wie persönlich.
Antje Peukert danke ich für ihre wunderschöne Freundschaft, sie hat mir bei vielen Gelegenheiten sehr geholfen und mich unterstützt.
Ich möchte mich gerne bei allen Kollegen bedanken, die meine Arbeit leichter gemacht haben: Michael Böttcher für seine Hilfe bei der Entwicklung des Mikrochips, Christine Mißler für ihre Hilfe mit dem Konfokalmikroskop, Narayanan Madaboosi, Armin Renner für ihre Hilfe Zellen umzusetzen und Felix Jorde, Michael Kirschbaum, Katja Uhlig, Cristian Marschner, Thomas Leya, Andreas Lankenau, Thomas Zacke und alle andere KollegInnen des Fraunhofer Instituts.
Ganz besonders möchte ich Maria danken, die immer und nicht nur in den drei Jahren meiner Promotion mit mir war und meinen anderen Freunden Viviana, Sara, Adrian, Marton, Nicola, Christian, Deibris, Paula, Silvà, Albrecht und Kerstin, Malte und Sabine und meinen Geschwistern Riccardo und Diana.
Der größte Dank gilt meinen Eltern für die Weitsicht, mit der sie mich erzogen haben. Ich danke Ihnen für ihr Zutrauen und für alles, was sie mir gegeben haben, um heute ein glücklicher Mensch zu sein. Ihr Stolz gibt mir Kraft und Mut immer neue Türen aufzuschieben.

Erklärung

Hiermit erkläre ich, dass ich die vorliegende Dissertation selbständig verfasst und keine anderen als die angegebenen Quellen und Hilfsmittel benutzt habe. Ferner versichere ich, dass ich diese Dissertation noch an keiner anderen Universität eingereicht habe, um ein Promotionsverfahren zu eröffnen. Ich habe mich auch früher um keine Promotion bemüht.

Abstract

The mechanical properties and the deformation behavior of biological cells are mainly determined by the cytoskeleton. These properties are closely linked to many biophysical and physiological events of the cells, and may thus be exploited as potent biomarkers.
In this thesis we propose a new, advantageous approach to characterize cellular mechanical properties: Through the application of dielectrophoretic forces, different types of cells are stretched between microelectrodes.
The investigations are divided into four parts.
The first part deals with the comparative application of our newly developed dielectrophoretic stretcher to cell lines that have been derived from malignant and non-malignant tissues. Small numbers of human cells of cancerous origin (MCF-7) and from related non-cancerous tissue (MCF-10A) were sufficient to obtain data that allowed to unambiguously distinguish these cells. By applying our technique to malignant (L-929) and non-malignant (3T3) mouse fibroblast cells, we observed a deformation response to the electric field that confirmed the results obtained from the human cells. In both cases, nonmalignant cells turned out to be softer than their malignant counterparts. A detailed analysis of the dielectric properties of the human cells using dielectrophoretic spectroscopy showed that the differences in the stretching response are due to cell-specific mechanical properties and do not originate from differences in the polarizability. In order to deduce which parts of the cytoskeleton of the two cell types are mainly responsible for the different stretching behavior, an actin- and a microtubule-specific toxin were added to the cancerous and non-cancerous cells. Specific microtubular structures of the two cell types were identified as the major cause for the behavior observed.
The second part of the investigation focuses on the influence of aging culture medium on the mechanical properties of suspension cells HL-60. Our experiments clearly showed that the cellular stiffness is influenced by the cultivation duration. The results suggested that the changes in the stiffness of the HL-60 cells were primarily attributable to nutrient depletion of the culture medium over time. In contrast, the influence of changing pH value could be excluded as a potential factor responsible for the different deformation.
The third part of this work concerns the analysis of the chip heating induced by the electric field. The temperature distribution on the chip measured by using infrared thermography and a subsequent numerical calculation showed that our system produces a negligible temperature increment in the voltage and buffer electric conductivity range chosen for the experiments. The technique is thus suitable for working with biological cells.
In the last part, the investigation deals with the visualization of cytoskeleton struc-

tures during stretching by the electric field. We employed fluorescent labeling of the cells through GFP transfection. The results of these experiments demonstrated that our technique is compatible with optical investigation of internal structures of the cell. This allows studying the behavior of the cytoskeleton during mechanical deformation without causing damage to the cells.
Finally, the integration of our dielectrophoretic stretcher into a microfluidic system was realized and is described in this thesis.
Our approach shows enormous potential for parallelization and automation and, hence, should be suited to achieve throughputs that make it attractive for numerous biomedical diagnostic purposes.

Zusammenfassung

Die mechanischen Eigenschaften und das Deformationsverhalten biologischer Zellen werden hauptsächlich durch das Zytoskelett bestimmt. Diese Eigenschaften sind eng mit vielen biophysischen und physiologischen Ereignissen der Zelle verbunden und könnten deshalb als mächtiger Biomarker dienen.
In dieser Arbeit stellen wir einen neuen, vorteilhaften Technick vor, um die mechanischen Eigenschaften von Zellen zu charakterisieren: Durch die Anwendung dielektrophoretischer Kräfte werden verschiedene Typen von Zellen zwischen Mikroelektroden gedehnt.
Die Untersuchungen sind in vier Teile gegliedert:
Der erste Teil behandelt die komparative Anwendung unseres neu entwickelten dielektrophoretischen *stretchers* an Zellinien, die aus bösartigen und gutartigen Gewebe gewonnen wurden. Geringe Mengen menschlicher Zellen krebsartigen Ursprungs (MCF-7) und aus verwandtem nicht krebsartigen Gewebe (MCF-10A) reichten aus, um Ergebnisse zu erhalten, die eine eindeutige Unterscheidung dieser Zellen erlaubten.
Bei der Anwendung unserer Technik auf bösartige (L-929) und gutartige (3T3) Zellen aus Mausfibroblasten beobachteten wir eine Deformationsreaktion auf das elektrischen Feld, die die an den menschlichen Zellen beobachteten Ergebnisse bestätigten. In beiden Fällen stellten sich gutartige Zellen als im Vergleich zu ihrem bösatigen Pendant weicher heraus. Eine detaillierte Analyse der dielektrischen Eigenschaften der menschlichen Zellen durch Anwendung der dielektrophoretischen Spektroskopie zeigte, dass die Unterschiede bei der Dehnung durch zellspezifische mechanische Eigenschaften und nicht durch unterschiedliche Polarisierung verursacht werden.
Um aufzuklären welche Teile des Zytoskeletts der beiden Zelltypen hauptsächlich für das unterschiedliche Dehnverhalten verantwortlich sind, wurden den bösartigen und den gutartigen Zellen ein aktin- und ein mikrotubuli-spezifisches Toxin hinzugefügt. Spezifische Mikrotubulistrukturen beider Zelltypen wurden als Hauptursache für ihr Verhalten beobachtet.
Der zweite Teil der Untersuchungen konzentrierte sich auf den Einfluss alterndes Kulturmediums auf die mechanischen Eigenschaften der Suspensionszellen HL-60. Unsere Experimente zeigten eindeutig, dass die Festigkeit der Zellen durch die Dauer der Kultivierung beeinflusst wird. Die Ergebnisse deuteten darauf hin, dass Veränderung der Festigkeit der HL-60 Zellen primär auf den Nährstoffabbau im Kulturmedium über die Zeit zurückzuführen waren. Im Gegensatz dazu konnte der Einfluss eines veränderten pH-Wertes als potentiell verantwortlicher Faktor für eine veränderte Deformation ausgeschlossen werden.
Der dritte Teil der Arbeit befasst sich mit der Analyse der durch das elektrische

Feld verursachten Erwärmung des Chips. Der Temperaturverteilung auf dem Chip, gemessen durch Infrarotthermographie und eine anschließende Berechnung des Temperaturverlaufs zeigte, dass unser System unbedeutende Temperaturerhöhungen in dem für die Experimente gewählten Spannungsbereich sowie dem elektrischen Leitfähigkeitsbereichs des Puffers, erzeugt. Die Technik ist demnach geeignet, um mit biologischen Zellen zu arbeiten.
Im letzten Teil beschäftigen sich unsere Untersuchungen mit der Visualisierung der Zytoskelettstruktur während der Dehnung im elektrischen Feld. Wir benutzen eine Fluorenzenzmarkierung der Zellen durch GFP-Transfektion. Die Ergebnisse dieser Experimente demonstrieren, dass unsere Technik mit optischen Untersuchungen der internen Strukturen der Zelle voll kompatibel ist. Dies könnte die Erforschung des Verhaltens des Zytoskeletts während mechanischer Deformationen erlauben, ohne die Zelle dabei zu beschädigen.
Schließlich wurde die Integration unseres dielektrophoretischen *stretchers* in ein Mikrofluidiksystem realisiert und in dieser Arbeit beschrieben. Unsere Technik zeigt enormes Potential für die Parallelisierung und Automatisierung und sollte sich demzufolge für hohe Durchsätze eignen, die sie für zahlreiche biomedizinische Diagnosen attraktiv machen.

Contents

CHAPTER 1

Introduction

With the advent of the evidence-based medicine the importance of biomarkers has been steadily growing during the past years.
The term biomarker was defined by the National Institute of Health (NIH) as "a characteristic that is objectively measured and evaluated as an indicator of normal biological processes, pathogenic processes, or pharmacological responses to a therapeutic intervention."
Some of these biomarkers have the potential to speed up the process of diagnosis, others to provide a means of monitoring the state of progression of common diseases (e.g. cancer, heart disease and infection) and the effectiveness of therapeutic measures.
The pharmaceutical companies have also become increasingly interested in biomarkers and in the significant role that they play in pharmaceutical research and drug development processes.
Because of considerable disease heterogeneity, interpatient variation and other irrelevant sources of biological variability, biomarker discovery is extremely chal-

lenging.
Biomarkers can be specific cells, molecules, genes, gene products, enzymes, or hormones, or other indicators of the physiologic state and also of change during a disease process.
At protein level, distinct changes occur during the transformation of a healthy cell into a diseased cell, including altered expression, differential protein modification, changes in specific activity, and aberrant localization. In recent years, proteomic technologies allowed for the relatively accurate identification of these protein changes caused by the disease process and, thus, set the pace for biomarker discovery.

In biology and medicine, we tend to focus on the importance of genes and chemical factors for control of tissue physiology and the development of disease, whereas we commonly disregard physical factors. On the other side, biologists have recently come to recognize that the viscoelastic properties and deformation behavior of cells play important roles in many biophysical and biological responses [1, 2], and that they are equally potent as chemical cues [3]. Thus, the identification of mechanical biomarkers that can be used as surrogate measures of cell phenotype in different states of a disease, transformation, or differentiation has earned interest.

The link between biomechanics and human diseases has been the subject of considerable scientific research effort for a number of decades. The application of traditional solid and fluid mechanics concepts from physics and engineering to the study of biological and physiological problems has provided valuable insights into the mechanics of organ function and of processes associated with blood flow through the vasculature, the mechanical response of tissue, joints and articulating surfaces. Consequently, such approaches have also been adapted, with appropriate modifications, to model mechanical deformations of biological cells and subcellular components such as the cytoskeleton.
In the light of these trends and developments, the study of the cellular, subcellular, and molecular mechanics in human disease, including cancer, has emerged as a topic of rapidly expanding scientific interest in recent years. A particular focus of research in this area is to explore the connections among cellular state and cytoskeletal properties, biological function, and human health/disease state. Eukaryotic cells generally contain three types of polymer biomolecules as structural elements in the cytoskeleton: actin microfilaments, intermediate filaments and microtubules. This internal scaffolding determines the shape and the mechanical characteristics of the cell [2, 4]. The structure of the cytoskeleton was demonstrated to be transformed, for instance, by cancer [5]. Thus, altered protein structures also change the ability of cancer cells to contract or stretch. This can explain the existing link between cell deformability and cellular state. Consequently, parameters of the mechanical properties of cells could be used as indicators of their

biological state. An example of systematic studies about the influence of the disease state on single-cell and cell-population biomechanics is found in the in vitro study of the effects of the malaria-inducing *Plasmodium falciparum* on the deformability of human red blood cells (RBC) [6, 7]. Another target of this research field are the biomechanics and biophysics of cancer cells in order to establish a link between the deformability of cancer cells and cell signaling, cytoadherence, migration, invasion, and metastatic potential.

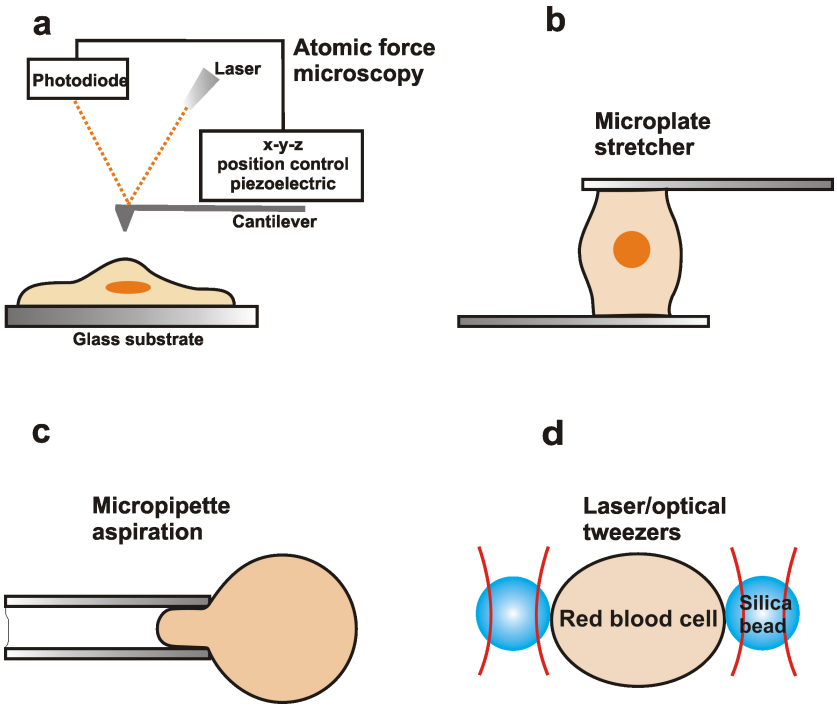

Figure 1.1: . a) Atomic force microscopy, b) microplate stretcher, c) micropipette aspiration and c) laser/optical tweezers. This figure is adapted from [6].

A variety of experimental methods has been used to extract the mechanical properties of healthy cells and their diseased counterparts. Figure 1.1 provides a schematic description of the main experimental techniques for living cells. In Figure 1.1-a, atomic force microscopy (AFM) is shown. In AFM, local deformation is induced on a cell surface through physical contact with the sharp tip at the free end of a cantilever [8, 9]. Figure 1.1-b-c-d show mechanical microplate stretcher (MS), micropipette aspiration (MA) [10, 11] and optical tweezers (OT) [7, 12], respectively. With these methods, forces can be induced on the whole cell while the submicrometer deformation is monitored optically.
In the particular case of the mechanics of cancer cells, noteworthy examples are the microplate stretcher to deform human pancreatic epithelial cells [13, 14] and

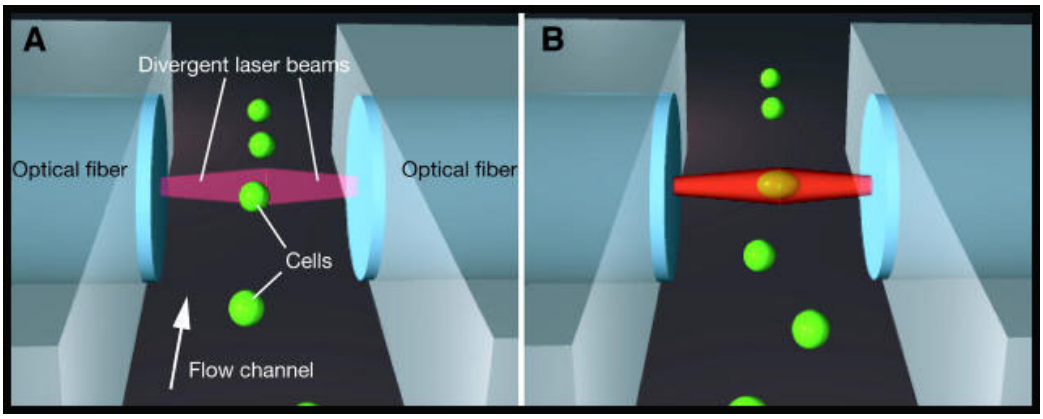

Figure 1.2: Schematic representation of the optical stretcher. A. The cells flowing in the channel are trapped by the two divergent laser beams. B. When the cell is centered, a higher laser power is employed to stretch it. This figure is taken from [16].

the optical stretcher that was employed for deforming nonmalignant and malignant human breast cells [15]. The microplate stretcher relies on a proper adherence of the cells to the plates, whose displacements impose the stretching. On the contrary, for the characterization of the cells using the optical stretcher, adherent cells are trypsinized and used in spherical form. Then the cells flow in a microchannel where they are trapped and stretched by two laser beams (Fig. 1.2). This method has been demonstrated to provide data on the viscoelastic properties of cells at a considerable processing speed. The information obtained can be used to distinguish cells according to several biomedically relevant criteria [16].

In this thesis, we propose a new approach to characterize the mechanical properties of cells. Our newly developed dielectrophoretic stretcher analyzes cells by deforming them using dielectrophoresis, i.e. by exerting electric forces between two electrodes.

The term dielectrophoresis (DEP) was first introduced by Pohl [17] to describe the translational motion of particles due to a force exerted on them when they are subjected to a non-uniform electric field. This motion is determined by the magnitude and polarity of the charges induced in a particle by the electric field [18].

After the pioneering work on the viscoelastic properties of erythrocytes in the group of Sackmann [19], dielectrophoresis has mainly been applied on microchip dimensions to position, direct and separate a variety of biological cells including bacteria, yeast and mammalian cells [18, 20].

In this thesis, we determine the stiffness difference between different cell types through dielectrophoresis.

In the gap between two electrodes, the cells undergo an elongation through the interaction of charges at the interface between cell and buffer with the electric field.

As already mentioned above, it is well-known that the cellular deformability depends on the cell type and on several parameters that reflect the cell state. After establishing our method through the analysis of well-characterized cell lines, we aim at using it for the evaluation of unknown cell samples for diagnostic purpose. We applied our technique to cell lines that have been derived from malignant and nonmalignant cells of both human breast cells and animal fibroblast cells. Mesenchymal cells and senescent suspension cells were also analyzed by this method. In order to perform single-cell analysis in micrometer format, we have designed a microchip in which a single cell from a given population can be brought and stably trapped into a position where the analysis is then carried out.
The cell lines of malignant and non malignant human cells used in our experiments were two well-known and widely used, closely related cell lines: MCF-10A, a non-tumorigenic epithelial cell line derived from benign breast tissue with fibricystic disease, and MCF-7, a corresponding line of human cancer cells, namely adenocarcinoma. Their mechanical deformability was studied in order to establish whether it is possible to distinguish between these two cell types according to their malignancy degree.
The extent of deformation of the cells by the electric field is attributable to the mechanical properties of the cellular internal structure as well as to their dielectric properties, i.e. internal and membrane electric conductivity and permittivity. Therefore, both factors were analyzed separately. In order to analyze the dielectric properties of the cells we used the dielectrophoretic spectroscopy analysis, as described in [21, 22]. By chemical modification of the cytoskeleton, we analyzed the individual contributions to the deformability of actin filaments and microtubules and identified which component is responsible for the differences in deformability between malignant and nonmalignant cells. Additionally, we used our stretcher to characterize two fibroblast cell lines: 3T3 and L-929 cells. It is known that these two fibroblast cell lines show different tumorigenic behavior, namely 3T3 cells can be considered nonmalignant and the L-929 malignant [23–25]. The aim of these experiments was to observe whether the fibroblast cells showed similar malignant-nonmalignant feature to the human breast cell lines when they were stretched by an electric field.

Suspension cells were also investigated. The suspension cell lines that we used in our experiments were HL-60, U937 and Jurkat cells, which are myeloid leukemia, histiocytic lymphoma and T lymphocyte cell leukemia, respectively. By applying our novel technique, we demonstrated that their mechanical properties are related to the aging of their culture medium. These three cell lines showed different degrees of stiffness when deformed by the electric field, but all showed a sensitivity to the depleted medium. A complete analysis of the HL-60 cells was performed to determine whether shifts in the pH value or nutrient depletion was responsible for the change of the mechanical properties of the cells over time.

The visualization of the mechanical structures inside living cells and of the influence that the electric field has on them was also one of our targets. We transfected the cells using tubulin-GFP in order to visualize the microtubules. Then we stretched the cells, while monitoring the behavior of these cytoskeletal structures.

The detailed analysis of the dielectrophoretic stretcher, presented in this thesis, is motivated by a number of advantageous features such as:

- it can be easily combined with dielectrophoretic units for aligning, sorting and positioning single cells so that entire single-cell processing lines can be established in a chip format
- the dielectrophoretic approach is well-suited for miniaturization because of the relative ease of microscale generation and structuring of electric fields on microchips
- microelectrodes can now easily be processed in microfluidic environment at comparably low cost. Together with the low energy demands for driving electrodes, this feature enables highly parallel processing. This aspect is facilitated through the progress that has recently been achieved with respect to the integration of electrodes into microsystems such as lab-on-chips [26].
- by reducing the scale of the electrode size, a strong reduction of the operating voltage to produce the same DEP force on a particle is obtained. Since the DEP force is proportional to the spatial gradient of the squared electric field ∇E^2, an *n*-fold change in electrode scale results in an operating voltage change of $n^{3/2}$. For 100-fold reduction of electrode size, a 1000-fold reduction of operating voltage will therefore produce the same DEP force on the cells [26]. The practical advantage is a significant reduction in electric heating and electrochemical effects. The electrode design determines the surface to volume ratio of DEP elements and, thus, its efficiency of heat dissipation, which is, according to the Fourier's law, inversely proportional to the electrode size [27].
- the label-free characterization offers the advantage of minimal interference with the natural state of the cells and reduces the number of necessary steps in the process, like washing, blocking etc, thus, opening up the potential for high cell troughput
- the simple set-up permits easy access of optical detection schemes
- the analysis is accomplished at a single cell level, ensuring that the entire information content can potentially be obtained. Studies made at the

single-cell level are not affected by the averaging effects characteristic of bulk-phase population-scale methods. Thus, they offer a level of discrete observation that is unavailable with traditional methods, in which the information of the individual cellular response is lost in the bulk average (Fig. 1.3).

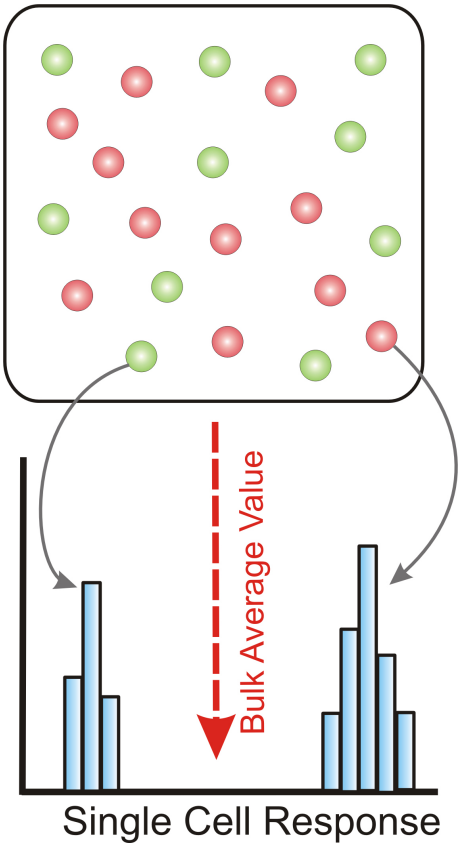

Figure 1.3: Example of misleading results obtained when analyzing blended responses of a bulk cell population due to its heterogeneity. Bulk measurements only provide average values of the population and are not suitable for determining the contribution of individual cell species.

These considerations lead us to assess that our dielectrophoretic stretcher can be a suitable and favorable technique to analyze the mechanical properties of cells.

CHAPTER 2

Theoretical background

Dielectrophoresis exploits the dynamic effects of non-uniform electric fields on dielectric, i.e. poorly conductive, and in most cases uncharged objects. It should not be confused with electrophoresis which is the motion of an electrically charged particle induced in an electric field. The applied field can be direct current (DC) or alternating current (AC). For technical as well as biological reasons, AC electric fields are usually preferred [28].
In this chapter the basic parameters and equations are considered in order to describe the dielectrophoretic behavior of a biological cell in an AC electric field.

2.1 Dielectric properties of cells

One of the important subjects of the biophysics is the investigation of the dielectric properties of cells and the structural part of them (membrane, cytoplasm, etc.). These properties can provide valuable information about the cellular architecture, its functions, and metabolic mechanisms. For the analysis of the dielectric prop-

erties of cells several classical models are usually used. On the one hand, the cell model has to be simple enough to permit the calculation of the electric field distribution in the cell and in the surrounding medium. On the other hand, it should reflect the basic electric properties of the cell that determine its specific polarization processes. In the simplest case, the model consists of a homogeneous conductive sphere (cytoplasm), surrounded by a thin homogeneous shell (cell membrane) having a small conductance. This so called single-shell model correctly describes the main polarization processes occurring at the boundaries between the cell membrane and the internal and external media [18]. According to this model, the cell can be described by two parameters - permittivity and conductivity.

Whereas the conductivity σ is a measure of the ease with which mobile charges can move through the material under the influence of the electric field, the permittivity ε reflects the extent to which immobile charge distributions can be polarized under the influence of the electric field.
The permittivity can be expressed as a complex function in the form:

$$\varepsilon^* = \varepsilon^{'} - j\varepsilon^{''} \tag{2.1}$$

in which the imaginary factor may be defined in terms of a frequency-dependent conductivity as

$$\varepsilon^{''} = \frac{\sigma(\omega)}{\omega\varepsilon_0} \quad \text{thus,} \quad \varepsilon^* = \varepsilon - j\frac{\sigma(\omega)}{\omega\varepsilon_0}. \tag{2.2}$$

The factor ε_0 is the dielectric permittivity of free space and has the value 8.854 x 10^{12} Fm^{-1}.
Up to the Mhz range, the permittivity ε of biological particles is relatively high and then typically decreases with increasing frequency in three major steps (i.e. dispersions) which are designated as α-, β-, and γ-dispersions (Fig. 2.1). The β-dispersion is the most relevant in our experiments and it can be interpreted as interfacial polarization. Its physical basics will be detailed in the next section. The two other dispersions are associated with other effects, which are not of interest in this context and will not be dealt with in this thesis.

2.1.1 Single cells in an external electric field

The passive electric properties of a spherical cell in a liquid medium can be described by a simplified electric circuit (Fig. 2.2). The membrane is represented by a capacitor (C_m) in parallel with a resistor (R_m) that simulate the membrane conductivity (G_m). In DC fields and low frequency AC fields the conductivities of the external and internal media can be described by simple resistors (R_{ex1}, R_{ex2}, R_{in}). R_m is by orders of magnitude higher than R_{ex} and R_{in}. Therefore, a low frequency current does not flow through the cell, but around it [29]. Thus, because

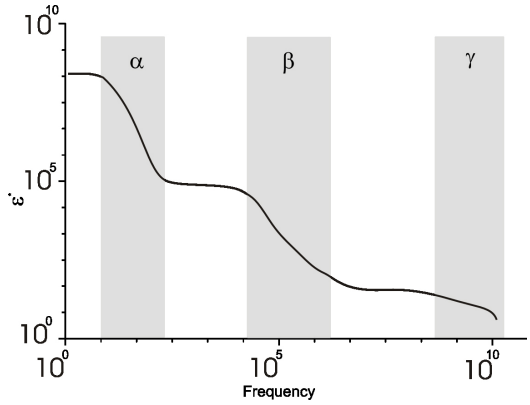

Figure 2.1: Schematic illustration of the three frequency-dependent regions of α-, β-, and γ-dispersion [29].

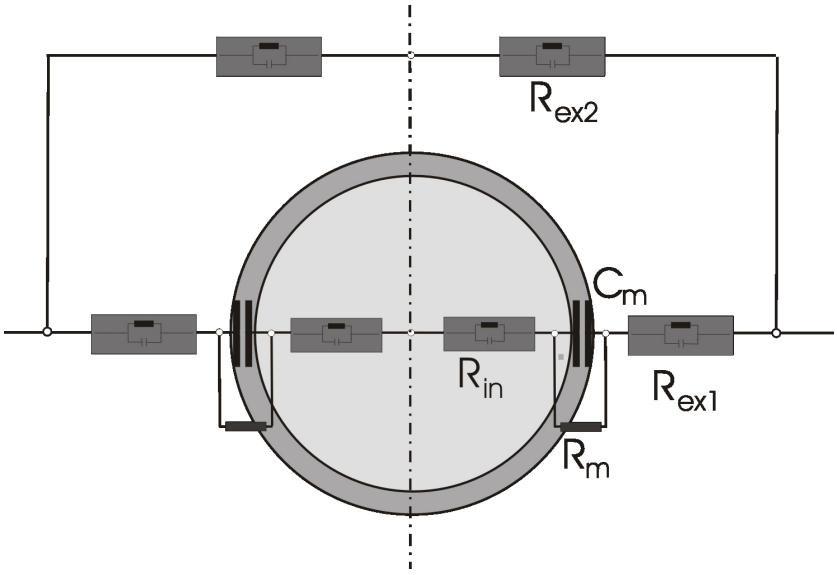

Figure 2.2: Simplified analog circuit demonstrating current ways through and around a spherical cell. R_{ex1} R_{ex2} are the resistances of the external medium. R_{in} is the resistance of the cytoplasm and R_m, C_m the resistance and the capacity of the membrane, respectively. This figure is adapted from [29].

of the high membrane resistance, in DC fields and extremely low frequency AC fields, the resistance of the cell membrane insulates the cell interior (cytoplasm) from the external electrical field and no current is induced within the cell interior. The external field becomes deformed (Fig. 2.3). When the frequency of the external field increases, the membrane capacitor becomes short-circuited and this

allows the electric field to penetrate into the cell. Thus the effective permittivity and conductivity of a cell will respectively fall and rise with increasing frequency, leading to the existence of a dielectric dispersion, the β-dispersion (see Fig. 2.1). If there is no large difference in the permittivities between the medium and the cytoplasm, the amount of field penetrating the cell depends only on the relation of the inside-outside electric conductivities.

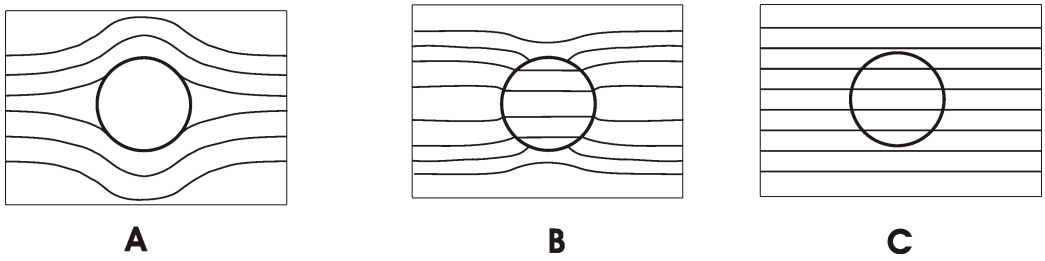

Figure 2.3: Field lines for a spherical cell in an electric AC field. A. The cell in a low frequency range. B. The cell in an AC field of intermediate megahertz frequencies. The conductivity of the external medium is lower than that of the internal one. C. The cell in a high-frequency range (f >100 MHz). The polarization of the cell is negligible when the permittivities of the internal and external space are the same. The figure is adapted from [29].

2.1.2 Dielectrophoretic force

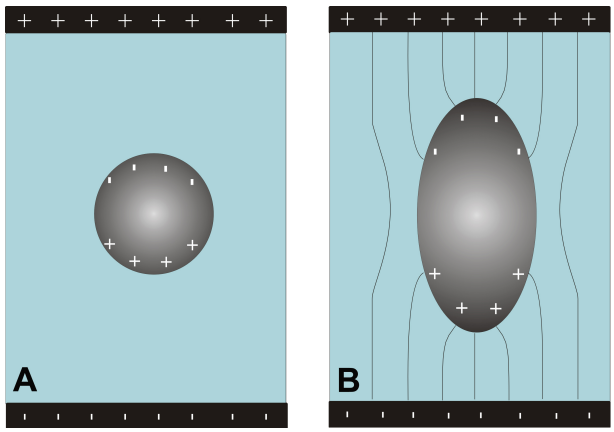

Figure 2.4: Schematic representation of the polarization of a cell in an electric field. If the electric field is homogeneous two forces act on the charges that cause a stretching of the cells in the field direction.

Pohl was the first to use the term dielectrophoresis. He demonstrated that when an AC electric field acts on a dielectric particle (e.g. a biological cell),

a dipole moment is induced within the particle. The dipole moment *m* induced in the cell can be represented by the generation of equal and opposite charges (+q and -q) at the particle boundary. If the field is inhomogeneous the induced charges of the dipole are located at different positions and the local electric field, and its resulting strength, is shown to vary. Thus, the polarized particle experiences a translational force, known as dielectrophoretic force, the magnitude and direction of which depends on the electrical properties of the particle and its surrounding medium [17]. Thus, depending on the relative polarizability of the cell with respect to the surrounding medium, it moves either towards the high-electric field region (positive dielectrophoresis, pDEP) or towards the region where the field is weaker (negative dielectrophoresis, nDEP). This force also depends on the magnitude and frequency of the applied electric field. For spherical particles, the time-average dielectrophoresis (DEP) force is

$$F_{DEP} = 2\pi r^3 \varepsilon_0 \varepsilon_m Re[K(\omega)] \nabla \left|E_{rms}\right|^2 \tag{2.3}$$

[29] where *r* is the particle radius, ε_0 is the permittivity of the free space, ε_m is the real part of the permittivity of the surrounding medium, and E_{rms} is the root mean-square electric field. The factor $K(\omega)$ (the Clausius-Mossotti factor) depends on the complex permittivity of both the particle and the medium and is a measure of the effective polarizability of the particle. In the presence of high-frequency (kHz-MHz) electric fields, the polarizability of a cell is a complex function of the field frequency [30]. In the case of spherical particles, this factor is given by

$$K(\omega) = \frac{\sigma_p^* - \sigma_m^*}{\sigma_p^* + 2\sigma_m^*}, \qquad \sigma_{i,i=p,m}^* = \sigma_i + j\omega\varepsilon_0\varepsilon_i \tag{2.4}$$

[29] where the indexes *p* and *m* refer to the particle and the medium, respectively. The parameters ε and σ are, respectively, the permittivity and the conductivity of the dielectric, ω is the angular frequency of the applied field ($\omega = 2\pi f$), and $j = \sqrt{-1}$. The DEP force is proportional to the square of the applied field strength. This results from the double role of the electric field: on the one hand it induces the dipole, on the other hand, it drives the particle. As already mentioned above, particles can experience two dielectrophoretic effects.

Positive dielectrophoresis: Re[K(ω)] >0 (or $\sigma_p > \sigma_m$). Particles are attracted to electric field intensity maxima and repelled from minima.

Negative dielectrophoresis: Re[K(ω)] <0 (or $\sigma_p < \sigma_m$). Particles are attracted to electric field intensity minima and repelled from maxima [31]. For spherical particles, -0.5 <Re[K(ω)] <1.

If the electric field is homogeneous and $\sigma_p > \sigma_m$ the dipole, the forces $\vec{F}_x = +q\vec{E}_{rms}$ and in the negative x-direction $\vec{F}_{-x} = -q\vec{E}_{rms}$ act on the charges. The two forces cause a stretching of the cells along the field direction (Fig. 2.4) [32–34].

2.1.3 Crossover frequencies

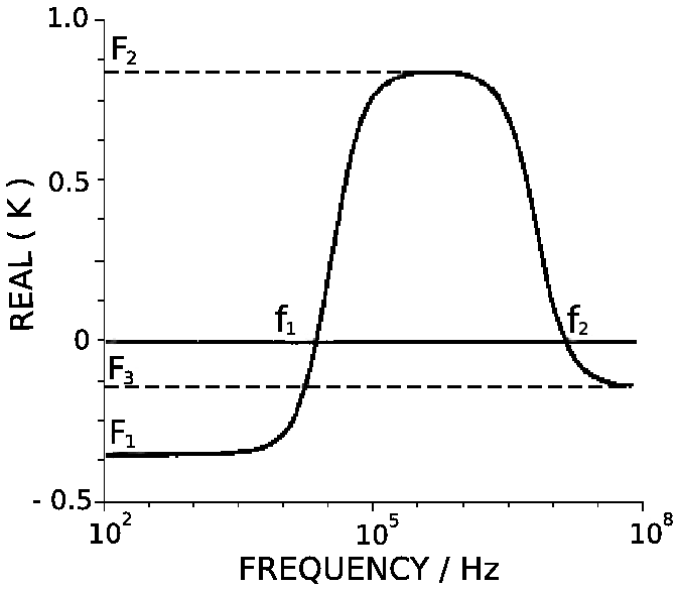

Figure 2.5: Typical dielectrophoretic spectrum for a single-shell model. Five characteristic points of the spectrum are defined.

As explained above, the dielectrophoretic force is proportional to the real part of the dimensionless parameter K (eqn. 2.4). An exemplary dielectrophoretic spectrum is shown in Figure 2.5. Each spectrum has five characteristic parts: three different plateaus of the force (F_1, F_2 and F_3) acting on the particle in different ranges and two critical frequencies (f_1, f_2) called crossover frequencies. At these frequencies the dielectrophoretic force ceases to exist [18]. The first critical frequency f_1, at which DEP turns positive, is governed by the dielectric parameters of the cell membrane, i.e the area-specific membrane capacitance C_m and the area-specific membrane conductivity G_m. The second cross-over frequency f_2 defines the second transition and mainly depends on the dielectric parameters of cytoplasm, i.e. ε_{in} and σ_{in}.

2.2 The cytoskeleton

Cells have to organize themselves in space and interact mechanically with their environment. They have to be correctly positioned, physically robust, and properly structured internally. They have to be able to rearrange their internal components as they grow, divide, and adapt to changing circumstances. Many of them also

have to be able to change their shape and migrate. All these organizations are developed to a very high degree in eukaryotic cells and they depend on a remarkable system of filaments called the cytoskeleton [35]. The self-organization of three protein classes into specific filaments provides the structural and functional basis of the cytoskeleton. Each type of filament has distinct mechanical properties and dynamics, but certain fundamental principles are common to all of them.

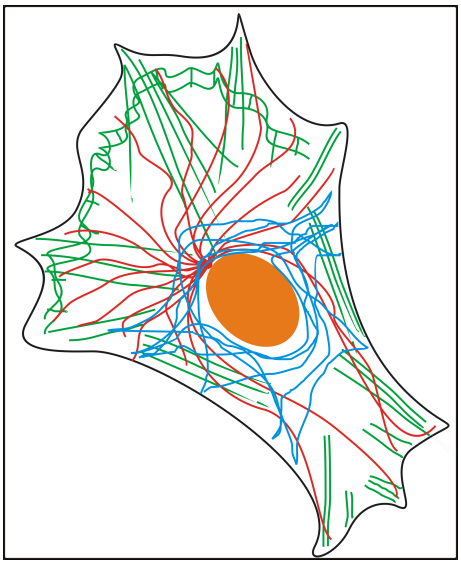

Figure 2.6: Schematic representation of the cytoskeletal filaments of an adherent cell. The actin filaments are arranged into parallel bundles and as a network under the cellular membrane (green filaments). The microtubules in most cells extend outward from a microtubule-organizing center, the centrosome, positioned near the nucleus (red filaments). The intermediate filaments are scattered throughout the cytoplasm and concentrated around the nucleus (blue filaments).

- *Actin filaments* are thin flexible protein filaments with a diameter of about 8 nm and composed of the protein actin. They are cross-linked into a dense three-dimensional meshwork beneath the plasma membrane, or they can be more regularly arranged into parallel bundles. Actin filaments determine the shape of the cell's surface and are necessary for whole-cell locomotion. They provide the highest resistance to deformation up to a certain critical value of local strain [35].

- *Microtubules* are long strands of the protein tubulin, they are relatively thick and inflexible. They have a hollow cylindrical form with an outer diameter of 25 nm and a lumen diameter of 10 nm and they are the most distinctive cytoskeletal components in the central region of the cytoplasm. The microtubules determine the positions of membrane-enclosed organelles and direct intracellular transport. As to their mechanical properties, microtubules do not have sufficient tensile or shear stiffness to significantly impart integrity to the cytoskeleton. Individual microtubules have been considered resistant to large scale compression.

- *Intermediate filaments* often have a similar distribution in the cell to microtubules, but are readily distinguishable from the latter by their smaller diameter, which is close to 10 nm. They are irregular flexible ropes of protein and composed of a large family of proteins. They terminate on the matrix of the proteins embedded in the nuclear envelope and radiate out from there into the surrounding cytoplasm. They are sufficiently compliant to allow moderate deformation, and yet they maintain their resistance to shear deformation at large local strains [36, 37].

The shape of the cell and its ability to move depend on a large retinue of accessory proteins that form the links between the principal filaments and the other structural elements. These accessory proteins contribute significantly to the strength of a cytoskeleton. The structural architecture of the cytoskeleton is the basis for the mechanical properties of cells, exhibiting passive and active responses to deformations.

2.3 Relevant viscoelastic models

The concept of stress is related to the strength of the material. If the cross-sectional area of the object is A and the force acting in the object is F, the ratio

$$\sigma = \frac{F}{A} \tag{2.5}$$

is the *stress* in the object. The basic unit of stress in the International System of Units (SI units) is *newton per square meter* (N/m^2) or *pascal* (Pa).
The deformation of a body that can be related to stresses is described by strain. In this thesis the dimensionless ratio

$$\varepsilon = \frac{l - l_0}{l_0} = \frac{\Delta l}{l_0} \tag{2.6}$$

will provide a measure of the deformation.

Classical models. Figure 2.7 shows three mechanical models, the *Maxwell model*, the *Voigt model* and the *Kelvin model*. All of these are composed of combinations of linear springs and dashpots. A linear spring is supposed to produce an instantaneous deformation proportional to the load. A dashpot produces a velocity proportional to the load at any instant. For the Maxwell body, the sudden application of a load induces an immediate strain by the elastic spring, followed by creep of the dashpot,that is the body continues to deform. The same reaction is reflected also in the unloading process. For the Voigt model, a sudden application of force produces no immediate deflection, because the dashpot, in parallel with

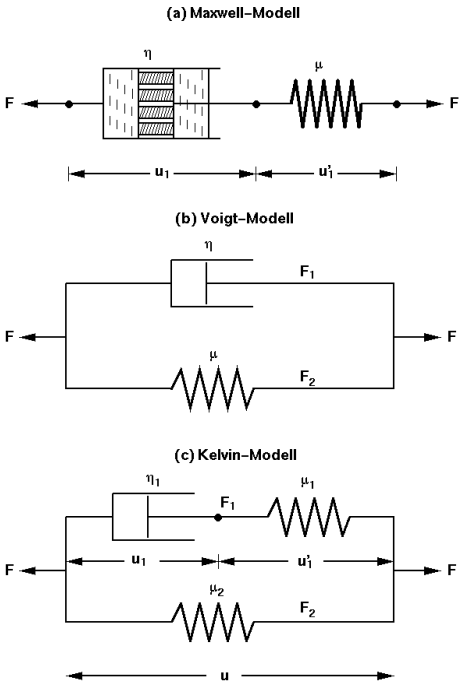

Figure 2.7: Three models of viscoelastic materials. (a) A Maxwell body, (b) a Voigt, and (c) a Kelvin body (standard linear solid). Maxwell introduced his model, implying that all fluids are elastic to some extent. Kelvin showed the inadequacy of the Maxwell and Voigt models in accounting for the rate of energy dissipation in various materials subjected to cyclic loading. Kelvin's model is commonly called the standard linear model because it is the most general relationship.

the spring, does not move instantaneously. Instead, as can be seen in Figure 2.8 a deformation is gradually built up, while the spring takes a greater and greater share of the load. In the unloading process the dashpot displacement relaxes exponentially. The Kelvin model has simultaneously the properties of elastic body and viscous fluid. It has the properties of the sudden change of strain, the residual strain and the creep.
If the body is subjected to a cyclic loading, the stress-strain relationship in the loading process is different from that in the unloading process, and the phenomenon is called *hysteresis* [38].

Stress-strain test. The stress-strain curve is an extremely important graphical representation of a material's mechanical properties. At low strain, many materials show elastic behavior, so the stress is proportional to strain. As strain is increased, many materials eventually deviate from the linear proportionality. This non-linearity is usually associated with stress-induced "plastic" flow in the specimen. Here the material is undergoing a rearrangement of its internal molecular or microscopic structure, in which molecules are being moved to new equilibrium positions. These microstructural rearrangements due to plastic flow are usually not reversed when the load is removed, in other words the material exceeds the elastic limit. Elasticity implies the complete and immediate recovery from an imposed displacement on the release of the load, and the elastic limit is the value of

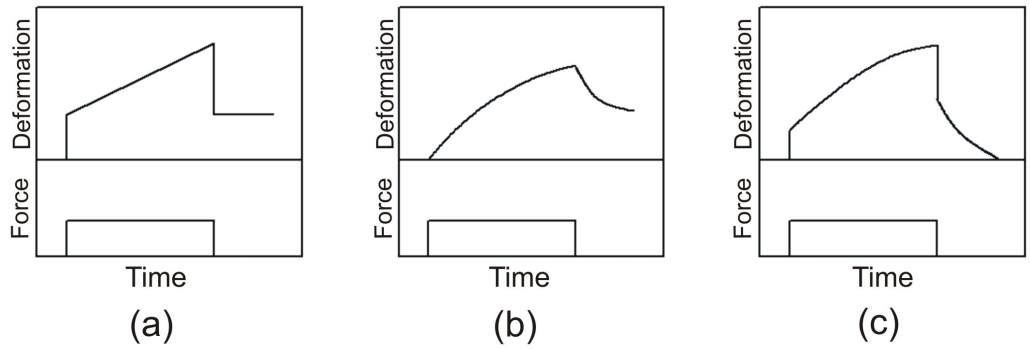

Figure 2.8: Creep function of (a) a Maxwell, (b) a Voigt, and (c) a Kelvin model.

stress at which the material experiences a permanent residual strain that is maintained upon unloading. A closely related term is the yield stress G_p. This is the stress needed to induce plastic deformation in the specimen.

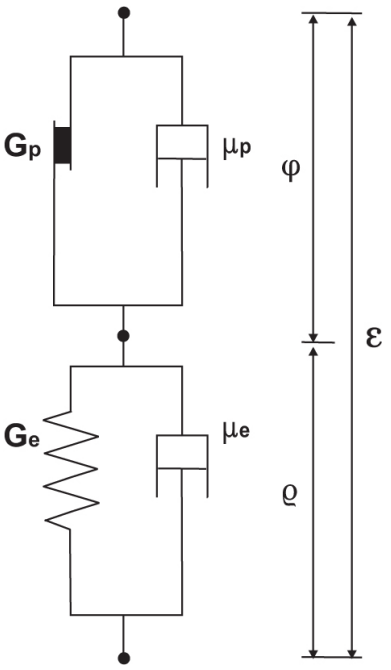

Figure 2.9: Structure of the model that satisfies the essential features of the cellular response in the experiments. The model consists of a parallel viscoplastic element (*on the top*) in series with a parallel viscoelastic element (*on the bottom*). G_p = yield stress; η_p = viscosity in parallel with G_p; G_e = elastic modulus; η_e = viscosity in parallel with G_e. The deformation ε is the sum of deformations of the viscoplastic element φ and of the viscoelastic element ϱ.

Viscoplastic model. During the application of a force, the deformation of a biological cell is dependent on a combination of the cell's intrinsic elastic, vis-

cous and plastic properties. Simple considerations suffice to eliminate all classes of models with viscous and elastic elements, that have been proposed in section 2.3. The Kelvin model is widely used to represent the viscoelasticity of a body, but it always shows a full recovery and, thus, it cannot explain the deformation behavior of a cell. To qualitatively explain the behavior of the cells in response to the applied electric force, the mechanical model proposed by Butler and Kelly [39] is helpful. This mechanical arrangement is shown in Figure 2.9. Let *l* be a displacement of one of these elements. The deformation ε, when applied to these elements, satisfies the following relations:

- for the viscous elements $\sigma_v = \eta \frac{d\varepsilon}{dt}$
- for the elastic element $\sigma_e = G_e\varepsilon$
- for the plastic element $\frac{d\varepsilon}{dt} = 0$, for $|\sigma_p| < |G_p|$ and as long as $|\sigma_p|$ does not exceed the yield stress G_p

G_e is the elastic modulus, η is the viscosity and G_p the yield stress. The plastic element is rigid for deformations smaller than the yield stress, and cannot sustain any deformation greater than the yield stress. We will not go into more details of this model, since it was only intended to serve as a qualitative model of the response of cells subject to a deformation force and to provide an explanation of the deviation of their behavior from the classical models detailed in Figure 2.8.

CHAPTER 3

Materials and Methods

3.1 Cell cultures

In this study suspension and adherent cell lines were used.

3.1.1 Suspension cells

Human acute myeloid leukemia HL-60, human histiocytic lymphoma U-937 and human T cell leukemia Jurkat cell lines were obtained from the German Collection of Microorganisms and Cell Cultures (DSMZ, Germany). Standard procedures were followed for the cell cultures. The medium used for regular culture was 90% RPMI 1640 (with 2.0 g/l NaHCO, 25 mM HEPES, 5.5 g/l NaCl, 5 mg/l phenol red, and stable glutamine) supplemented with 10% fetal bovine serum (FBS). Cells were maintained in 25-cm^2 plastic flasks filled with medium under a 5% CO_2 : 95% air atmosphere at 37 °C in a humidified incubator. The appropriate amount of medium for covering the surface was $\sim$ 200 μl/cm^2. Every 2-3 days cells were

split: A fraction of the cell suspension (5 x 10^4 cells/ml) was introduced in a new flask with fresh culture medium. All cell culture reagents were from Biochrom AG (Berlin, Germany).

3.1.2 Adherent cells

MCF-7 human cells were kindly donated by Robert Clarke, University of Manchester, UK. MCF-10A human cells were obtained from American Type Culture Collection (Rockville,MD). 3T3 and L-929 mouse fibroblasts were obtained from DSMZ. Mesenchymal cells were kindly donated by Hagen Thielecke, Fraunhofer IBMT, St. Ingbert, Germany.
Cells were grown adhering on the bottom of 25-cm^2 culture flasks filled with medium and maintained under a 5% CO_2 : 95% air atmosphere at 37 °C in a humidified incubator.

MCF-7 and MCF-10A cell lines. MCF-7 is a human breast adenocarcinoma cell line. They were cultured in standard glucose Dulbecco's Modified Eagle's Medium (DMEM) (Gibco Invitrogen, Carlsbad, CA, USA), with 10% fetal bovine serum (FBS) (Biochrom AG, Berlin, Germany). Every 3-4 days cells were split. The culture medium was removed from the flask, cells were washed with Ca^{2+}, Mg^{2+} - free phosphate-buffered saline (PBS) in order to remove non-adherent cells and all traces of serum which contained trypsin inhibitor. This protocol was employed for splitting all adherent cell lines used in this work. 0.5 ml trypsin solution (Trypsin / EDTA 0,25% / 0,02%) was added and left for 13 minutes to detach cells. 3 x 10^5 cells in suspension were introduced in a new flask with fresh culture medium.

MCF-10A is a human non-tumorigenic epithelial cell line derived from benign breast tissue with fibrocystic disease. These cells are immortal, non-cancerous mammary epithelial cells. They were cultured in DMEM/F12 supplemented with 5% horse serum, 0.5 μg/ml hydrocortisone, 10 μg/ml insulin, 20 ng/ml EGF, 0.1 μg/ml cholera toxin, 2 mM glutamine and 1% Penicillin-Streptomycin [40–42]. After having applied the split protocol as above described, 1 ml trypsin solution (Trypsin / EDTA 0,05% / 0,02%) was introduced and left for 10 minutes to detach the cells. To neutralize trypsin 3 ml medium supplemented with FBS were added. 1 x 10^5 cells in suspension were centrifuged, the medium was removed and the cell pellet resuspended with fresh culture medium and introduced into a new flask. All cell culture reagents were from Gibco Invitrogen (Carlsbad, CA, USA).

3T3 and L-929 cell lines. 3T3 is a fibroblast cell line established from disaggregated Swiss albino mouse embryos. The cells were cultured in standard glucose Dulbecco's MEM with 10% FBS. The split protocol was applied as described above. 0.5 ml trypsin solution (Trypsin / EDTA 0,25% / 0,02%) was introduced

and left for 5 minutes to detach the cells.

L-929 are connective tissue fibroblast cells established from the subcutaneous areolar and adipose tissue of a mouse. They were cultured in standard RPMI 1640 medium with 10% FBS. The cells were splitted according the protocol described above. 1 ml trypsin solution (Trypsin / EDTA 0,05% / 0,02%) was added and after having wetted the whole surface, 0.8 ml were removed and the rest remained for 5 minutes to detach the cells.

3 x 10^5 cells of both 3T3 and L-929 cells in suspension were introduced in their respective new flask with fresh culture medium.

Mesenchymal cells. Mesenchymal stem cells are multipotent adult stem cells that can differentiate into a variety of cell types. These cells were directly obtained from biopsy samples from human knee tissue. They were cultured in Alpha MEM (with GlutarMAX, without ribonucleosides and deoxyribonucleosides) with 15 % FCS and 1 % Penicillin-Streptomycin. Every 3-4 days cells were supplied with fresh medium. Cells were split every 2-3 weeks, as they grow comparatively slowly. The culture medium was removed from the flask and the cells were washed with Ca^{2+}, Mg^{2+} -free PBS. Then 1 ml trypsin solution (Trypsin / EDTA 0,05% / 0,02%) was introduced and left for 3 minutes to detach the cells. 1 x 10^5 cells in suspension are introduced in a new flask with fresh culture medium. All cell culture reagents were from Sigma-Aldrich (US).

Use of the cells in the experiments. Before the experiments, the adherent cells were trypsinized in order to obtain a suspension of cells with spherical shape. The required aliquot of suspension cells was removed from the flask without any previous treatment. The appropriate quantity of cell suspension ($\sim$ 1 x 10^5 cells) was centrifuged and then re-suspended in an isotonic buffer. The buffer is a mixture of 0.3 M inositol solution with PBS and a 0.5 weight-% of a soluble polymer that effectively reduces non specific sticking of the cells to the microchip surfaces. The buffer components are from Evotec Technologies, Hamburg. The measured electric conductivity of the buffer was 5.5 mS/m (Conducting meter, Knick, Berlin).

3.2 Fluorescent staining procedures

Actin filaments of MCF-7 and MCF-10A cells were stained using Alexa Fluor Phalloidin 488 (Invitrogen, Germany). It binds to actin, preventing its depolymerization, and it is poisoning the cell. For staining of the cellular nucleus, we used DAPI (Sigma-Aldrich, US). In order to visualize the microtubules, the cells were transfected with pTagGFP-tubulin (BioCat, Germany), using FUGENE HD Transfection Reagent (Roche, Germany). The staining and the transfection were done according to the manufactures' instructions.

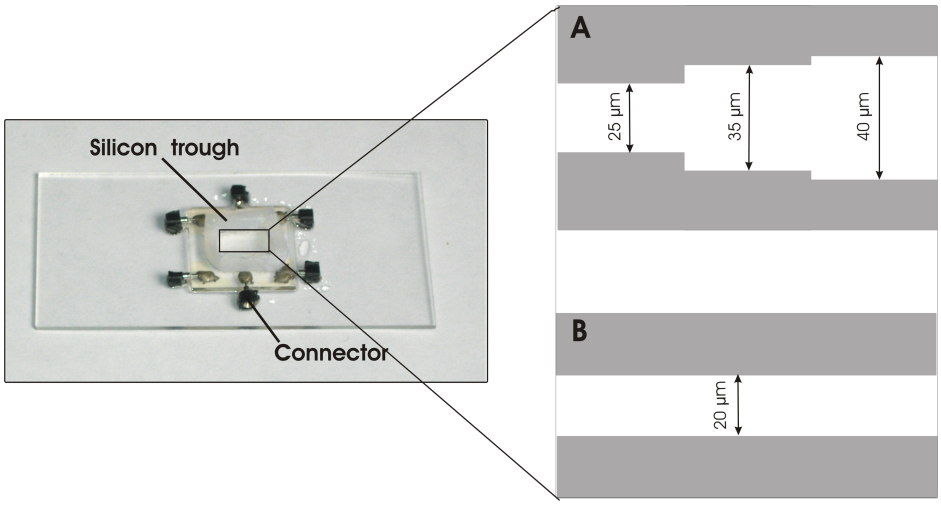

Figure 3.1: Microchip used for the experiments. Two different planar arrangements were designed. The arrangement A possesses three different gaps on the same structure. B. This arrangement was used for most experiments.

3.3 Microchip

The microchips used in the experiments consisted of two different planar arrangements of microelectrodes. The arrangement in Figure 3.1-A was used to test the feasibility of the technique. Afterwards, we only used the arrangement with parallel microelectrodes 20 μm apart. Both arrangements were made of indium tin oxide - a transparent conductive material - that was plated on glass slides (20 mm x 20 mm, Schott, Gruenenplan, Germany). All structures were prepared by UV laser ablation. The laser-ablation equipment is based on a system produced by Exitech. A KrF excimer laser (Lextra 100, Lambda-Physik Goettingen, Germany) produces a UV beam (248 nm) with a constant pulse duration of 10 ns. The structured glass slide was glued on a microscope slide in order to simplify handling for optical microscopy. The electric connectors were fixed on the microchip using an electrically conductive adhesive. To reduce buffer evaporation effects, silicone troughs with a volume of roughly 200 μl were mounted on the slides.

3.4 Modeling.

For the finite element simulation (Fig. 4.1), we used the Quasi-Statics Electric package from the Electromagneties Module of Comsol Multiphysics 3.2 (Comsol, Stockholm, Sweden). For this, the medium relative permittivity was set to 78.69

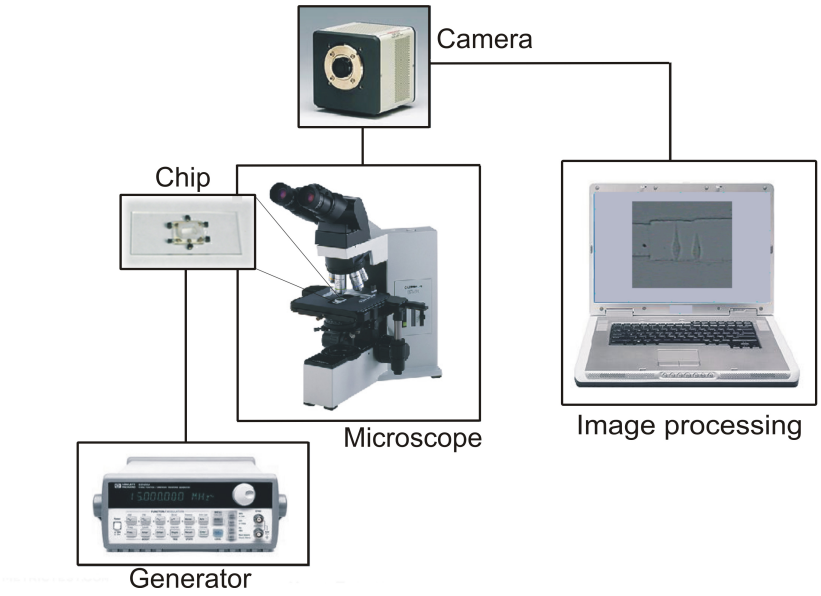

Figure 3.2: Experimental set-up used for the experiments

and its electric conductivity to 5 mS / m. The dielectrophoretic spectroscopy analysis simulation (Fig. 4.5) was performed using Mathematica 7.0.0 (Wolfram Research).

3.5 Experimental setup

3.5.1 Stretching experiments

Due to the simple construction of the microchip almost any optical method can be applied to investigate the cell stretching. The general experimental setup is sketched in Figure 3.2. Optical microscopy was performed using an Olympus BX40 microscope with a 20 x / 0.35 objective (Olympus, Hamburg). For recording the experiments a computer-controlled CCD camera (Orca ER, Hamamatsu Photonics Deutschland) was plugged to the microscope. The camera was controlled by the program Simple-PCI provided by the camera manufacturer. The chip electrodes were connected to a function generator that produced a 15 MHz signal and a square waveform (33120A, Agilent). The applied voltages were 4 V_{rms} for the experiments with suspension cells and of 6 V_{rms} with adherent cells (unless otherwise indicated below).

Image Processing The CCD camera provided a frame rate of nine digitized frames per second with 640x512 pixels^2. The images were converted to 8-bit resolution. The resolution of the stored images was 0.3 μm/pixel. The transient deformation amplitude of the cells was measured manually with the help of the software Image-ProPlus (Media Cybernetics, Inc.) usually every 2 seconds in the first 10 seconds of recording and then every 5 seconds after that for a total period of one minute.

3.5.2 Dielectrophoretic Spectroscopy

Dielectrophoretic spectroscopy was performed at different buffer conductivities. The chips used - as described above but made of platinum-plated glass and with a gap of 200 μm - were connected to a purpose-built high-frequency generator (Elektronik-Manufaktur Mahlsdorf EMM, Germany), which supplied frequency signals between 16 MHz and 400 MHz. Signals between 15 MHz and 20 kHz were produced by the function generator that we used for the stretching experiments (see above). The experimental set up, the data acquisition and the image processing were identical to what has been described under 3.5.1. Measurements were made at medium conductivities in the range from 0.001 to 0.9 S / m and crossover frequencies for at least six cells were determined for each conductivity. The different buffer conductivities were obtained mixing different ratios of the inositol solution and PBS.

Table 3.1: Parameters of heating analysis

Voltage	Buffer Conductivity	Gap width
0 V	5.5 mS/m	20 μm
1 V	0.3 S/m	35 μm
2 V	1.4 S/m	
3 V		
4 V		
5 V		

3.5.3 Chip heating

Evaluation of chip heating during the experiments was accomplished using an infrared camera PYROVIEW 3802 compact (DIAS Infrared GmbH, Dresden, Germany), that offers non-contact temperature measurements. Heating of the chips

with parallel microelectrodes was measured by positioning the chips under the infrared camera and monitoring the temperature distribution on the chip. The analysis was performed for different gap widths, different voltages and different buffer conductivities (listed in table 3.1). The two different electrode structures that were analyzed had a gap width of 20 μm and 35 μm. Each chip structure was immersed into a buffer with electric conductivity of 0.0055, 0.3 and 1.4 S / m, respectively, and connected to a generator that provided voltages between 0 and 5 V with intervals of one volt. For each parameter combination a thermal image was obtained, which was processed with Mathematica to obtain the maximum of the spatial temperature distribution. The measurements were accomplished at room temperature.

CHAPTER 4

Results and discussion

In this chapter we first describe our initial experiments, that we carried out to test the feasibility of the technique and to optimize the experimental arrangement. The main part of the chapter presents the results obtained from the electrically induced stretching of adherent and suspension cell lines. We address possible reasons underlying the observed differences in the stretching. We first analyzed the dielectric properties of adherent cells and secondly their cytoskeleton. Further, we investigated the influence of medium consumption on the cellular stiffness of suspension cells. Finally, we describe the visualization of the cytoskeleton structure of living cells during stretching. The last part of this chapter deals with the analysis of chip heating.

4.1 Dielectrophoresis in the microchip

After the application of the cell suspension to the silicon trough on the chip, the cells move randomly through the bulk liquid by convection. When they approach

the gap between the microelectrodes, the dielectrophoretic force attracts them towards the nearest electrode edge, where they come to a rest. The electric field between the electrodes induces the cell stretching [30, 32]. In Figure 4.1 a finite element simulation of the electric field acting on the cell is depicted. Figure 4.1-A shows the direction of the dielectrophoretic force towards the microelectrodes along the gradient of the electric field (eqn. 2.3). In Figure 4.1-B the electric field is visualized that stretches the cell along the electric field lines. The elongation is quantified in the following as the strain ε, i.e. the change in cell length Δl along the field direction normalized by the initial length l_0, according to eqn. 2.6

$$\epsilon = \frac{\Delta l}{l_0}. \tag{4.1}$$

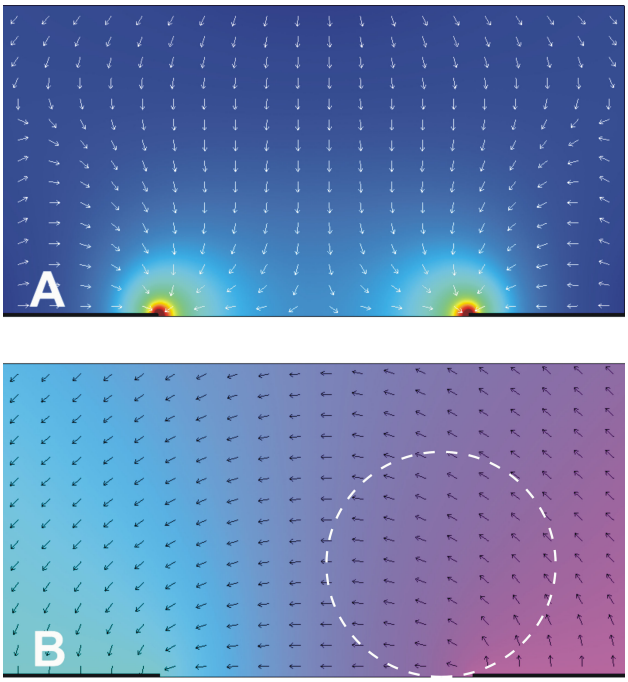

Figure 4.1: Finite element simulation of the electric field in the microchip. The electrodes are depicted by the black bars at the bottom of the drawings. A. The arrows indicate the direction of the dielectrophoretic force which transports the cells to the nearest electrode edge. The colors in the background indicate the electric field strength (bright colors, high field). B. The arrows show the direction of the electric field lines, along which a cell deforms (white dashed circle) at the right electrode. For a cell at the left electrode, the direction is exactly opposite. The background coloring codes the electric potential.

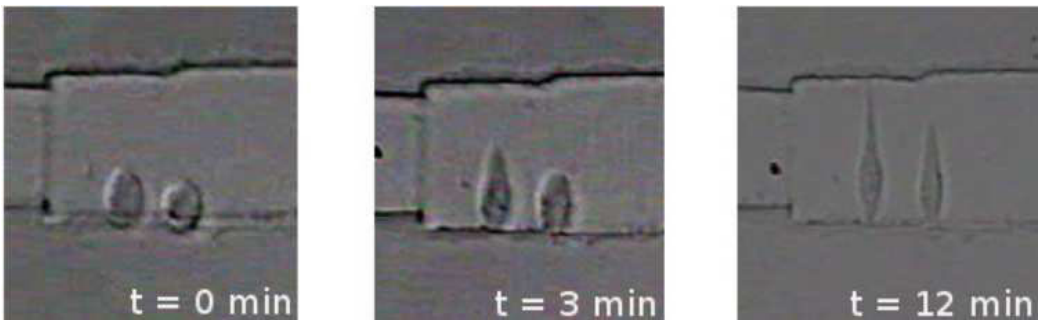

Figure 4.2: Qualitative feasibility test of the technique. Human leukaemia cells HL-60 were stretched for 12 min, yielding an elongation of more than 100%. This large elongation damaged many cells. Therefore, in the following experiments, either the gap between the electrodes or the exposure time were reduced (see page 38).

4.2 Validation of cell compatibility

The first part of this thesis deals with qualitative experiments to define an appropriate experimental set-up and a microchip design in order to obtain a suitable system for dielectrophoretic experiments and an easy monitoring of them. We first designed the chip with step-structure microelectrodes illustrated in chapter 3 (Fig. 3.1-A). The presence of three different gap widths was convenient for concurrently testing alternative electrode gaps. These tests were carried out with human leukaemia HL-60 cells. The cells were trapped at microelectrode edges with different gap widths and remained there for observation. In Figure 4.2 the resulting stretching is shown. With this experiment we verified that with our system it is possible to deform cells in an electric field and that the elongation is visible and measurable. The elongation increased further over time. After 12 min in the electric field, the cell vitality was tested by using trypan blue, a dye used to selectively stain dead cells blue. This test showed that the cells were vital after the electric stretching.
In order to optimize our experimental procedure, we were aming for (I) a high throughput of the cell analysis and (II) a reduction of potential side effects of the voltage used while maintaining an appropriate force to stretch the cells. The former could be achieved by minimizing positioning and stretching time. We believe that by reducing the gap width, the application of lower voltages is sufficient to obtain a high electric field to stretch the cells and it simultaneously limits the heating of the chip structure. Thus, for the experiments presented below we continued to use the microelectrode structure with parallel edges 20 μm apart (Fig. 3.1-B).

4.3 Stretching of adherent cell lines

4.3.1 Analysis of epithelial breast cells

To elucidate the relationship between the cellular state and the electric deformation, we investigated the well-defined cell lines MCF-7 and MCF-10A. They are widely used in breast cancer research, since MCF-7 cells provide an excellent in vitro model system to study human breast cancer and MCF-10A cells are frequently used as noncancerous control [43–45]. We have used MCF-10A cells instead of the widely used MCF-10F cells as MCF-10A is an adherent cell line. It represents the "natural" corresponding cell line to MCF-7.
The cell suspension was placed in the trough on the chip, which was connected to the generator. The generator was set to 2 V, which did not induce any measurable deformation, but served to attract the cells dielectrophoretically and to keep them in place. When the cell reached the gap between the two microelectrodes, the voltage was switched to 6 V for 60 s to stretch it. Each freshly prepared sample of cell suspension was used for the experiments at most for 20 min, in order to avoid anomalies of the cells caused by a deteroration of the culture conditions.
The elongation of the cancerous and the noncancerous cells during the application of the electric field for one minute is shown in Figure 4.3. The difference in the response of MCF-7 and MCF-10A cells is clearly visible in the comparison of their respective electric deformation. The MCF-10A cells emerge to be significantly softer than their cancerous counterparts. The two cell types are distinguishable already after few seconds and the difference in the electric deformability is significant after analyzing 25 cells. In order to obtain cell type characteristic parameters and to relate our response curves to previous work in the literature, fits to the experimental data obtained during force application have been performed. As a fitting function

$$\varepsilon(t) = p(1 - e^{-\frac{t}{\tau}}) + qt \tag{4.2}$$

has been chosen, since it is equivalent to solutions [46] of the constitutive equation used in [47]. The results of our experiments are represented in Figure 4.3-B and they were the following: The response time τ is similar for both cell types while

Cell line	τ	p	q
MCF-10A	(6 ± 1) s	(8.0 ± 0.7) x 10^{-2}	(1.2 ± 0.2) x 10^{-3}
MCF-7	(5.3 ± 0.8) s	(2.4 ± 0.3) x 10^{-2}	(0.5 ± 0.1) x 10^{-3}

p and q differ considerably. Our system proved to be a reliable method to distinguish between cancerous cells and their healthy counterparts. The experiments

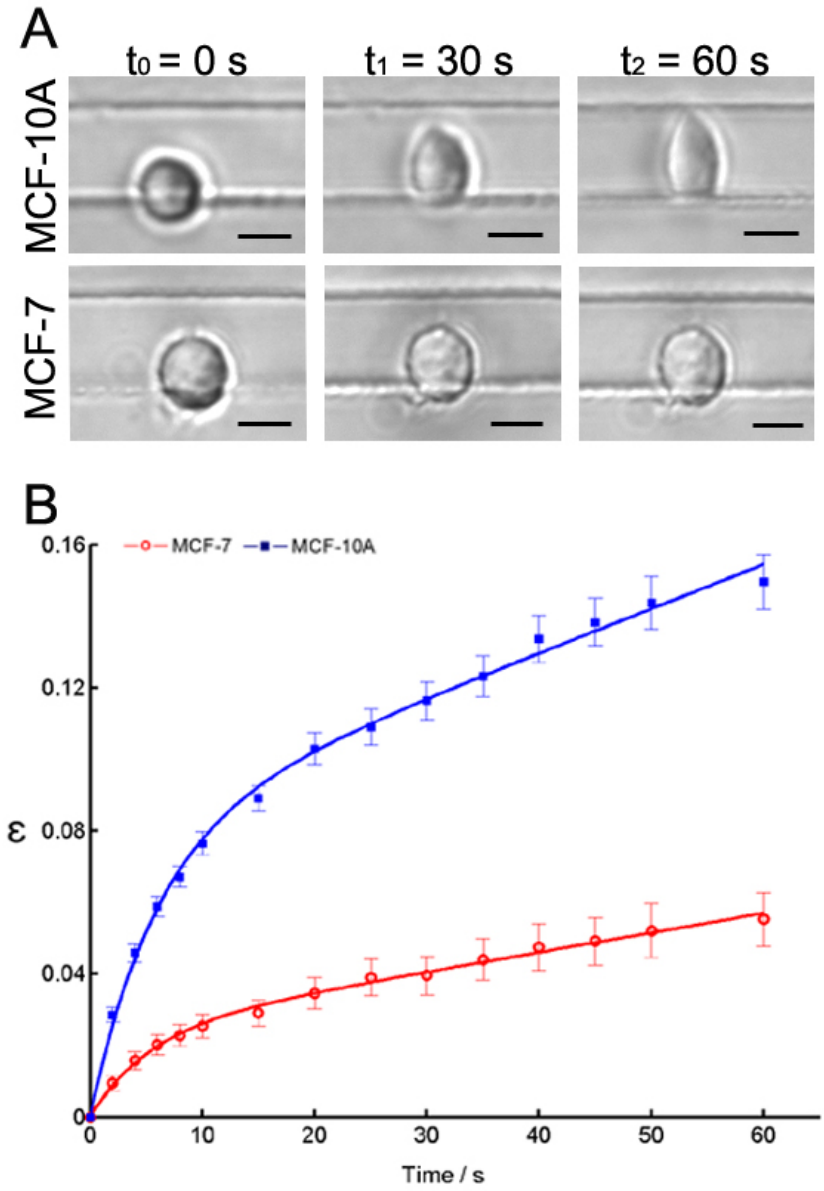

Figure 4.3: A. MCF-10A (top) and MCF-7 (bottom) cells during elongation due to electric field. The different stretching after one minute is clearly visible. Scale bar: 10 μm. B. Temporal evolution of the stretching of MCF-7 (open circles) and MCF-10A (solid squares) cells. The stretching behaviors are clearly different even in the first seconds (AC electric field amplitude 6V, frequency 15 MHz). The symbols and bars indicate average values and standard error obtained from at least 25 cells per cell type. The experimental data were fitted to the function 4.2

yielded reproducible results, that univocally showed the difference between the two cell lines.
To obtain an explanation of this phenomenon the determination of possible biological or physical reasons that could explain the difference in the electric elongation were addressed. The deformability of the cells in our system mainly depends on the two following factors:

- the stretching force that is determined by the dielectric properties, i.e. internal and membrane electric conductivity and permittivity as well as cell size
- the mechanical properties of the cell determined by the cytoskeleton structure

Both factors were individually analyzed to identify their respective contributions.

Analysis of dielectric properties. The idea of identifying cancer cells by their electrical properties is not new. In fact, it was first proposed by Fricke and Morse in 1926. It is well known that tumor tissues have significantly higher water content than their normal counterpart. For example, the water content of normal epidermis by weight is 60.9%, while that of carcinoma of the skin is 81.7%. Therefore, it is expected that tumor tissues exhibit somewhat larger permittivity and conductivity values than their homologous normal tissues [48]. On the other hand, the electrical conductivity and permittivity of biological materials will vary characteristically depending on the frequency applied.

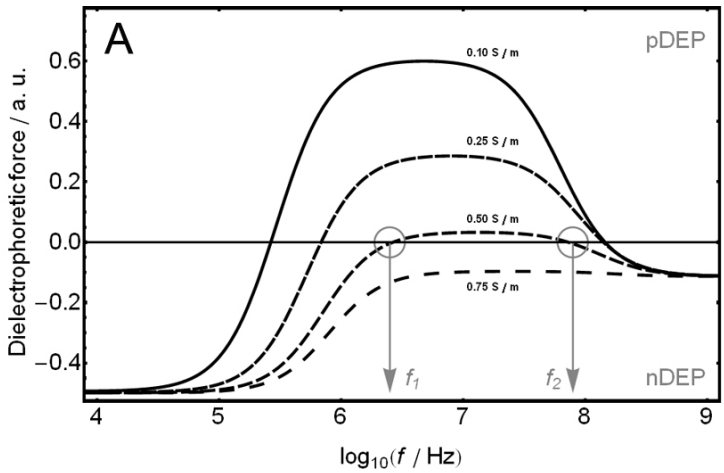

Figure 4.4: Dielectrophoretic force dependence on the external electric conductivity (σ_{ex}) for a model cell. The crossover frequencies f_1 and f_2 are depicted at different σ_{ex}, marked in the figure. (For the other parameters, see page 44)

We examined the dielectric properties of the MCF-10A and MCF-7 cells in a frequency window between 20 kHz and 400 MHz in order to check whether it is possible to distinguish them using their peculiar properties. For this purpose, we used dielectrophoretic single-particle spectroscopy, a non-invasive technique based on measuring the frequency dependence of the differences in electric polarizability between a cell and the surrounding liquid [49, 50]. Dielectrophoretic spectroscopy is a well-proven method, which is widely used to distinguish between cells or to detect cellular anomalies caused by a disease [18, 20, 51, 52].

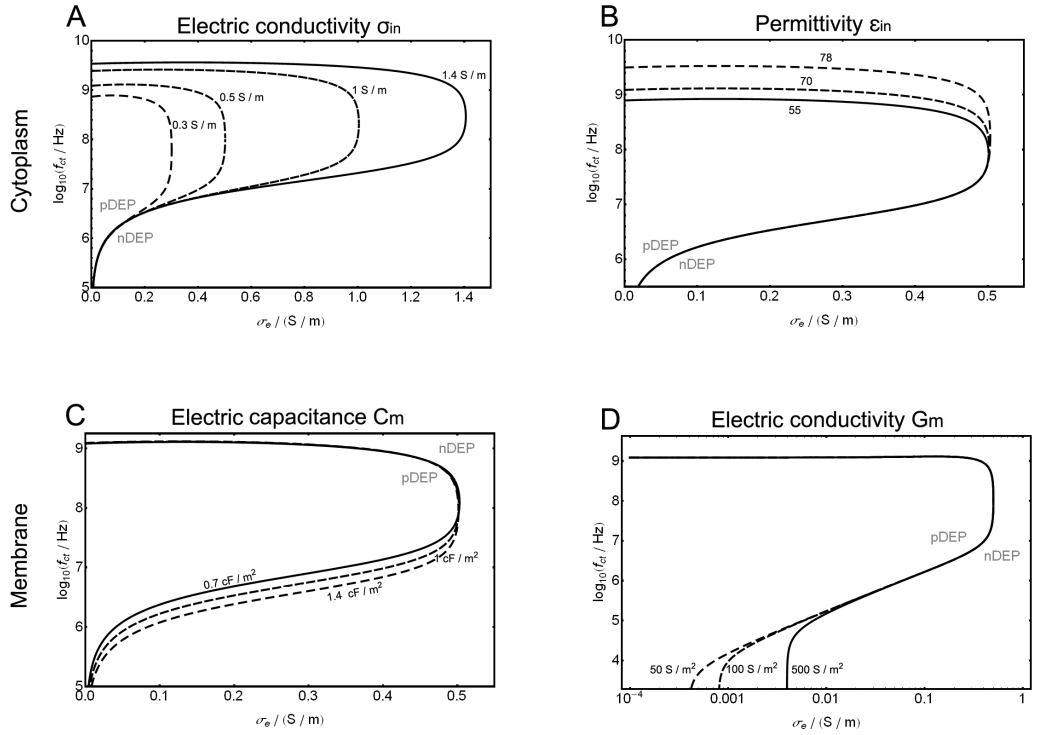

Figure 4.5: Dielectrophoretic single-particle spectroscopy of a model cell. The graphs show the external conductivity dependence of the crossover frequencies f_1 and f_2 (see fig 4.6-A). The high-frequency crossover f_2 is particularly sensitive to the dielectric parameters of the cytoplasm, while the lower frequency f_1 reflects the membrane polarization parameters. Variation of each cellular dielectric parameter (the internal permittivity ε_{in}, the internal conductivity σ_{in}, the membrane area specific electric conductivity G_m and the membrane area specific electric capacitance C_m) cause characteristic curve shifts. The values of the dielectric parameters used for the calculation are shown in the graphs. (For the other parameters, see pag. 44)

Under the influence of positive or negative DEP cells exhibit motion towards or away from electrodes edges. The DEP force turns from positive to negative or

vice versa at the crossover frequencies, defined as those frequencies at which cells experience zero DEP force. The values of the crossover frequencies depend on the medium conductivity and on the dielectric properties of the cells. Thus, measuring the crossover frequencies under varying external conductivity provides information on the cellular properties. As already mentioned in chapter 2, the lower frequency is primarily determined by the dielectric properties of the cell membrane (its electric conductivity and electric capacitance). The higher crossover frequency mainly depends on the dielectric parameters of the cytoplasm. In Figure 4.4 the crossover frequencies of a model cell with internal conductivity σ_{in} are depicted for different external conductivity values. The trend of these crossover frequencies gives information about the internal conductivity σ_{in}.
In the experiments that we carried out, the crossover frequencies were determined at different external conductivities by varying the frequency of the electric field and monitoring those frequencies at which the dielectrophoretic force vanished and the cell movement ceased. The experimentally obtained crossover frequen-

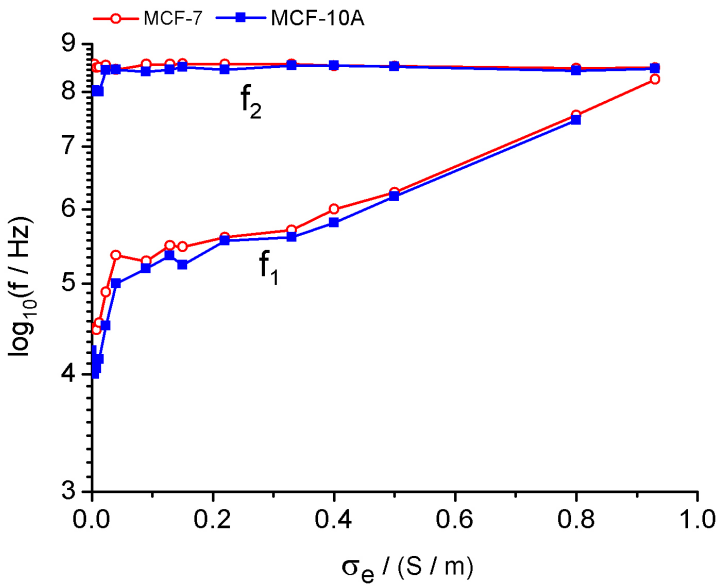

Figure 4.6: Experimental crossover frequencies of MCF-7 and MCF-10A cells as a function of the external conductivity. The two curves are highly similar without any significant difference between them. Thus, the differences in stretching (Fig. 4.3) cannot be explained by the dielectric properties of the two cell lines.

cies of the MCF-7 and the MCF-10A cells are plotted in Figure 4.6. The two branches that describe the lower (f_1) and the upper (f_2) crossover frequency are in very good agreement for MCF-7 and MCF-10A cells. Small deviations between the two cell types can be recognized at rather low conductivities, at around

100 kHz and at 100 MHz. The one at the higher frequency may be an artefact, although various measurements confirmed this sudden drop of f_2 for the MCF-10A. In order to evaluate the experimental data, simulations were carried out (Fig. 4.5) using a spherical body (cytoplasm) that is coated with a thin membrane as a model cell. The crossover frequencies were plotted as a function of the electric conductivities of the cytoplasm (σ_{in}) and the membrane (G_m), the permittivity of the cytoplasm (ε_{in}) and the capacitance of the membrane (C_m). In each case, all other parameters were held constant at the following values: cell radius 8 μm, specific membrane capacitance 0.01 F / m^2, medium relative permittivity 78.69, cytoplasm electric conductivity 0.5 S / m, cytoplasm relative permittivity 70, area-specific membrane electric conductivity 100 S / m^2. The simulations show that varying σ_{in} and ε_{in} has pronounced effects on the shape of the graphs, whereas changing the parameters associated with the membrane does not have a strong impact on the curve. Above a threshold external electric conductivity, only nDEP occurs. So, no crossover is detectable beyond this threshold.
The upper branch that represents f_2 which is rather close to f_{exp} = 15 MHz, the frequency used in the stretching experiments, does not change upon reasonable variation of the electrical membrane parameters. Comparing the two graphs in Figure 4.5-A-B with the simulations suggests that for both cell types the conductivity of the cytoplasm σ_{in} is approximately 1 S/m and the permittivity ε_{in} should be below 60. In this context, the dip of f_2 measured in the MCF-10A cells at low electric conductivity of the medium σ_{ex} should be inspected, since it occurs at values that are relatively close to the ones used for the stretching experiments (electric conductivity of the medium of σ_{ex} = 5 mS/m, and frequency of the electric field of f_{exp} = 15 MHz). According to the simulations, the dip should indicate a considerable change of σ_{in} and / or ε_{in} with decreasing σ_{ex}. We consider such a change implausible. In case the dip of the upper transition frequency f_2 of MCF-10A cells is actual fact, then f_2 would closely approach f_{exp}, resulting in a decrease of the Maxwell tension acting on MCF-10A cells. Hence, the contrast of stretching response between the two cell lines normalized to the force applied would be even stronger.

In conclusion, the two cell types are indistinguishable by this method, because both cell lines showed highly similar values of the crossover frequencies.

A further analysis was carried out in order to exclude the possibility that the dielectric properties are the determining factor for the stretching: the analysis of the cell velocity. When a cell is positioned in an electric field, the dielectrophoretic force of attraction to the electrodes is not the only force that is exerted on the cell. It is necessary to take into account the drag force F_F, which in our system is given by the Stokes law:

$$F_F = -6\pi\eta r v \tag{4.3}$$

where η is the viscosity of the fluid and v is the velocity of the cell with radius *r* relative to the surrounding fluid. Thus, the movement of the cell in a fluid is governed by:

$$F_{DEP} + F_F = m\dot{v} = F_{DEP} - 6\pi\eta r v \tag{4.4}$$

Integration of the equation 4.4 yields

$$v(t) = v_\infty(1 - e^{-\frac{t}{\tau_a}}) \tag{4.5}$$

where $v_\infty = v(t \to \infty)$ is the terminal velocity for the steady state. The characteristic time of acceleration τ_a is usually much smaller than the typical time of observation ($\sim$ 1 s). For a spherical particle of mass density ρ

$$\tau_a = \frac{2r^2\rho}{9\eta} \tag{4.6}$$

which is smaller than 10^{-6} s for cells and sub-micrometer particles. Therefore, the particle can be considered to move at its terminal velocity, given by

$$v_\infty = v(t \to \infty) = \frac{F_{DEP}}{6\pi\eta r} \tag{4.7}$$

This means that any measurement of particle velocity is a direct measure of the

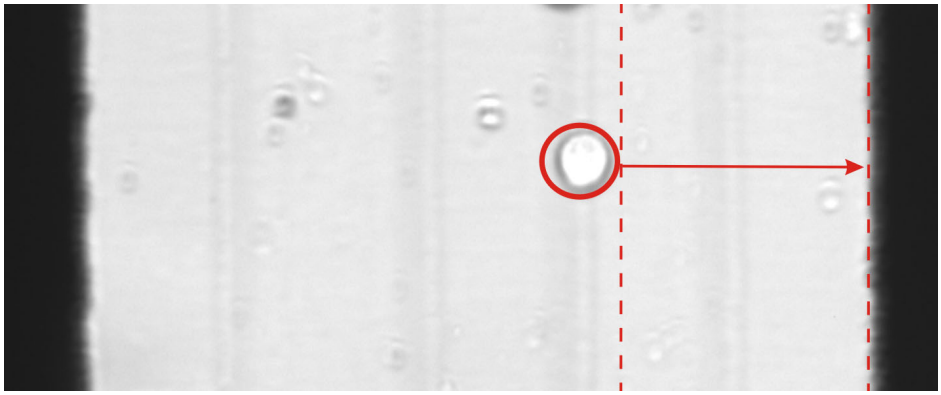

Figure 4.7: Analysis of cell velocity. Starting from a fixed distance, the time needed by MCF-7 and MCF-10A to reach the electrode structure (black edge) was measured and then compared to each other in order to achieve information about the dielectric properties of the cells.

velocity induced by the force acting on the particle, $\frac{F_{DEP}}{6\pi\eta r}$. In the light of the latter consideration, we measured the time that the MCF-7 and MCF-10A cells needed to travel a given distance (depicted with dashed lines in Figure 4.7) in order to

obtain their velocity. The dielectrophoretic force is the only variable parameter that can influence the terminal velocity in equation 4.7, because of its dependence on the permittivity and electric conductivity of the cells (see Clausius-Mossotti factor). Thus, different velocities would demonstrate that the cells have different dielectric properties. We measured the velocity of eight cells per type. Then we obtained the mean value (Fig. 4.8). Based on a Student's *t*-test, the two population

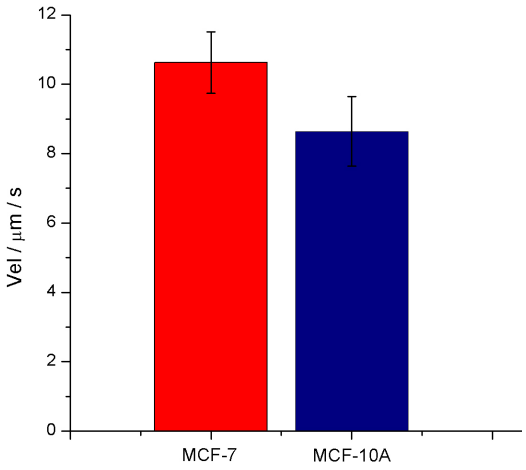

Figure 4.8: in the microchip for MCF-7 and MCF-10A.

are indistinguishable with 95% confidence. Therefore, the dielectric properties of the two cell types can be assumed to be similar to each other. Thus, in the frequency range observed, the differences in cell deformation are most probably not caused by the dielectric properties of cytoplasm.

Analytical calculation of the DEP force. In order to complete our analysis of the dielectric properties of the cells, we calculated the DEP force exerted by the electric field on the MCF-7 and MCF-10A cells by using data from literature [53]. The two decisive factors for the dielectrophoretic force are the real part of the Clausius-Mossotti factor Re[f_{CM}], determined by the inherent electric properties of the cells, the applied frequency, and the size of the cell. In fact, the DEP force is proportional to r^3 (eqn. 2.3), where r is the cell radius. Thus, r^3Re[f_{CM}] determines the DEP force. It is the crucial factor to distinguish cells according to their dielectric properties. In Figure 4.9 this factor is plotted for the two cell lines. The values of the electric conductivity of the cells are 0.3 S / m and 0.23 S / m for MCF-10A and MCF-7, respectively. The permittivity used in the calculation was 50 [54]. At high frequencies the force exerted on the MCF-10A cells is higher than the force on the MCF-7 cells, because the electric conductivity of the MCF-10A is greater than that of the MCF-7 cells. The higher electric conductivity

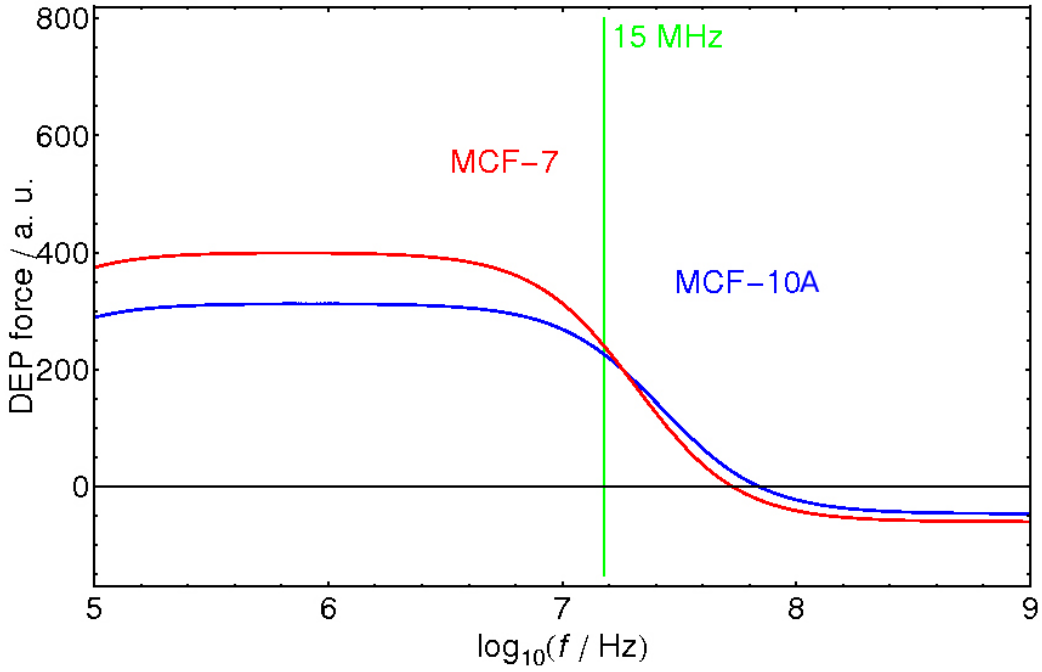

Figure 4.9: Calculation of the dielectrophoretic force acting on the two cell types.

of the MCF-10A cells continues to be the decisive factor down to frequencies of about 20 MHz. In this frequency range the MCF-10A cells are more polarizable than their diseased counterparts. At lower frequencies, however, the contribution through cell size dominates over the electric conductivity and MCF-7 cells experience a higher DEP force in comparison with MCF-10A cells, as the MCF-7 cells are bigger than the MCF-10A. Therefore, a certain frequency value exists where the curves intersect one another and at frequencies lower than this value the DEP force exerted on MCF-7 cells is decisively higher than that on MCF-10A cells. This behavior is strongly influenced by the cell size, which dominates the DEP force at low frequencies. The calculation shows that slightly above 15 MHz, which is the frequency value used in our experiments, the difference between the DEP force exerted on the two cell types is close to zero. Note, that 15 MHz was the maximum frequency provided by our generator. The factor $r^3\mathrm{Re}[f_{CM}]$ calculated for MCF-10A cells is 227.2 fl and that of MCF-7 cells is 242 fl. Thus, at 15 MHz the force acting on the MCF-7 cells is 6.5% higher than the force on the MCF-10A cells. This result confirms those of the other experiments described above, that were carried out in order to analyze the dielectric properties of the cells: Also in this simulation the difference in the polarizability between the two cell lines is not significant. In fact, in our experiments MCF-7 and MCF-10A deformed 6.2% and 14.3%, respectively, and, therefore, the effect of the DEP force

exerted on MCF-10A is 130% stronger than that on the MCF-7. This is a further indication that the difference in the deformation between the two cell lines is rather due to their different mechanical properties. This topic will be addressed in the next section.

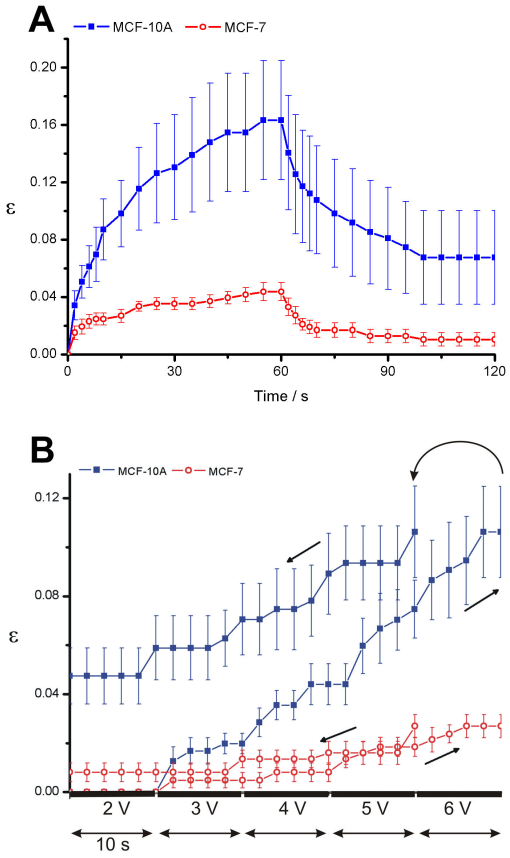

Figure 4.10: Elongation vs. field strength. A. Stress-strain curve with constant voltage for load and unload phase (6 V and 2 V respectively) for one minute per phase. The graphs resemble a spring-dashpot characteristic, refer to Figure 2.8. B. Stepwise increase of the voltage every 10 s to 6 V and analogous decrease to 2 V. The arrows indicate the step direction. In both cases, plastic and elastic deformation are observed.

Analysis of the cytoskeleton structure. The experiments described above indicated that the difference in deformation between the two cell types is not caused by the dielectric properties. The next step of our analysis was to investigate possible differences in the mechanical properties of the cytoskeleton. To characterize the behavior of MCF-7 and MCF-10A cells, stress-strain experiments were performed in two different modes: (I) a voltage of 6 V was applied for one minute, followed by 2 V for one minute. The latter voltage was again chosen to keep the

cells dielectrophoretically in place while it is too low to induce any measurable deformation. (II) The second mode utilizes a stepwise operation: the load is increased from 2 V to 6 V in steps of 10 seconds and 1 V each, followed by an analogous unload phase (Fig. 4.10).
The response of the cells indicates a damping that is caused by the structure of the cytoskeleton. This process was demonstrated by Wang [55] to be dependent on the mechanical interactions among all three filament systems. Wang also suggested that the permanent deformation might depend on chemical remodelling due to small cytoskeletal severing, and cross-linking and bundling of proteins, all processes associated with microfilament structures.
Both stress-strain experiments showed that the two epithelial cell lines differ in their mechanical response to the same applied stress. The two response curves in Figure 4.10 confirm what was already deduced from the stretching experiment (Fig. 4.3), namely that the strain response of the MCF-10A cell is approximately two and half times stronger than that of the MCF-7. Both cell types underwent a partially plastic deformation in the observation time. In both experimental modes, the relaxation part of the curves shows that 50 % of the strain relaxes in the case of MCF-10A cells, and approximately 70 % in the case of MCF-7 cells. The differences in the deformation response of the two cell types are thought to be caused by differences in the structure of the cytoskeletons. Consider Figure 4.10-B: During loading, the area under the stress-strain curve represents the strain energy per unit volume absorbed by the cell. Conversely, the area under the unloading curve is the energy released by the cell. In the elastic range, these areas are equal and no net energy is absorbed. But if the cell, as in this case, deforms plastically, the energy absorbed is higher than that released. This difference is a measure of the deviation from the elastic regime. Hence, it is clearly visible that the energy absorbed by the MCF-7 cells is less than that absorbed by MCF-10A cells, in accordance with the finding that they are stiffer than these nonmalignant ones.

Drugs-induced perturbations of the cytoskeleton. By the experiments described above, it was ascertained that the difference in the deformation response between the cancerous and noncancerous cells are caused by the differences of the architecture of the cytoskeleton. To gain insight into how the biopolymer filaments of the cytoskeleton contribute to the physical response of the cells, we performed stretching experiments in the presence of cytoskeleton-active toxins. Both cell lines were treated with either latrunculin A or colchicine, inhibitors of actin and microtubule polymerization, respectively [56–58]. The experimental data were fitted using the function in equation 4.2. These results are shown in Figure 4.11 and the fit parameters were:

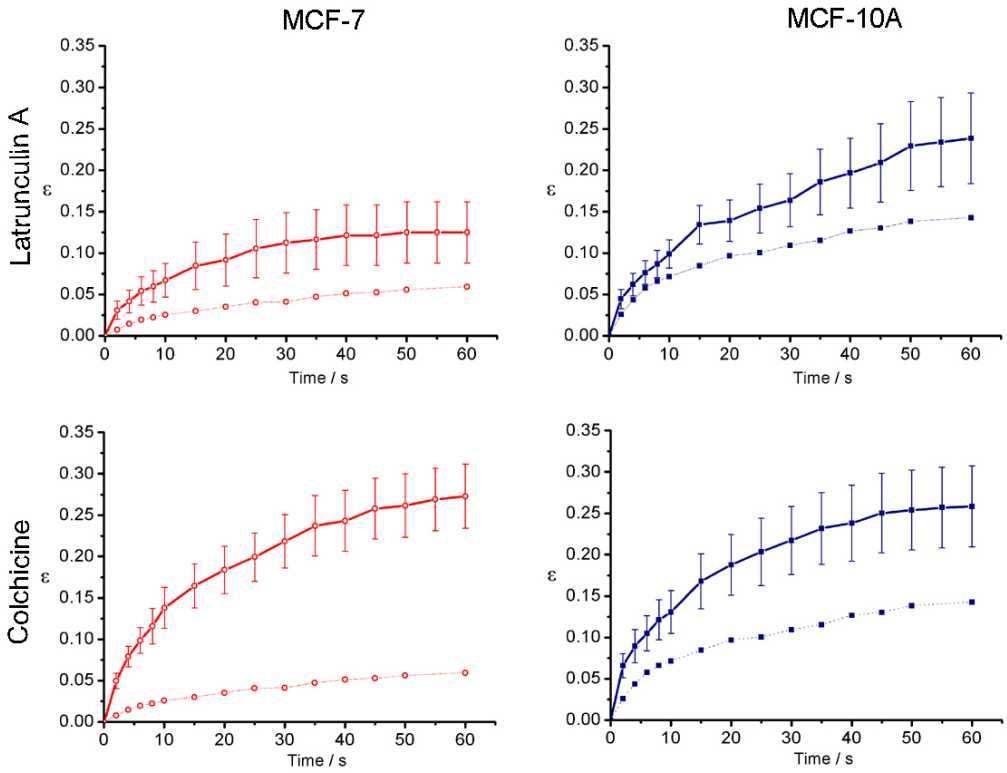

Figure 4.11: Drug-induced changes in the stretching behavior of MCF cells. (*Top*) Effect of latrunculin treatment (1 μM for 1 h). Both MCF-7 and MCF-10A cells became softer after the treatment and their respective maximum strain increases by about 110% for the MCF-7 cells and by 65% for the MCF-10A in comparison with that measured in the absence of the drug (dashed curves). Nonetheless, MCF-7 cells remain to be stiffer than MCF-10A cells without drug. (*Bottom*) Effect of colchicine treatment (2.5 μM for 2 h). The difference between the two cell types vanishes. This indicates a strong involvement of microtubules in causing a different response of the cells.

Latrunculin			
Cell line	τ	p	q
MCF-10A	(5 ± 1) s	(9 ± 1) x 10^{-2}	(2.6 ± 0.2) x 10^{-3}
MCF-7	(8.7 ± 1.7) s	(9.7 ± 1.2) x 10^{-2}	(0.5 ± 0.2) x 10^{-3}
Colchicine			
MCF-10A	(7 ± 2) s	(16.6 ± 1.8) x 10^{-2}	(1.7 ± 0.4) x 10^{-3}
MCF-7	(7.7 ± 1.1) s	(16.1 ± 1.4) x 10^{-2}	(2.0 ± 0.3) x 10^{-3}

As Figure 4.11 exhibits, after the latrunculin A treatment both MCF-7 and MCF-10A cells appeared considerably softer, i.e. the strain increased. Although the strain of MCF-7 cells increased by approximately 110 % and that of MCF-10A by 65 %, the MCF-7 cells remained stiffer than the MCF-10A cells, so that the difference in deformation was maintained. This experiment demonstrates that actin influences the response to mechanical deformation, but it is not the crucial component that determines the difference between the deformation of the two cell types in our system. In contrast, the colchicine treatment resulted in a softening of both cell lines such that the response of MCF-7 and MCF-10A cells to stretching became indistinguishable. These results indicate that in our case primarily microtubules are responsible for the differences in electric deformation.
Our analysis of the mechanical properties of MCF-7 and MCF-10A are in accordance with results reported in literature. Janmey [37] asserts that when the deformation of cytoskeletal microfilaments is measured under constant stress shear, F-actin can maintain an approximately constant strain for a long time in the presence of a relatively large stress shear. When the stress is relieved, F-actin recovers to very near by its prestress conformation. In contrast, microtubules were highly strained by a low stress, and the deformation increased significantly and continuously with time. Moreover, when the stress is removed, microtubules do not recover their prestrain shape, but rather exhibit unrecoverable strain characteristic of a viscous fluid. In the light of these considerations, it is safe to assume that the stretching in the MCF-7 and MCF-10A cells is mainly determined by the microtubules.

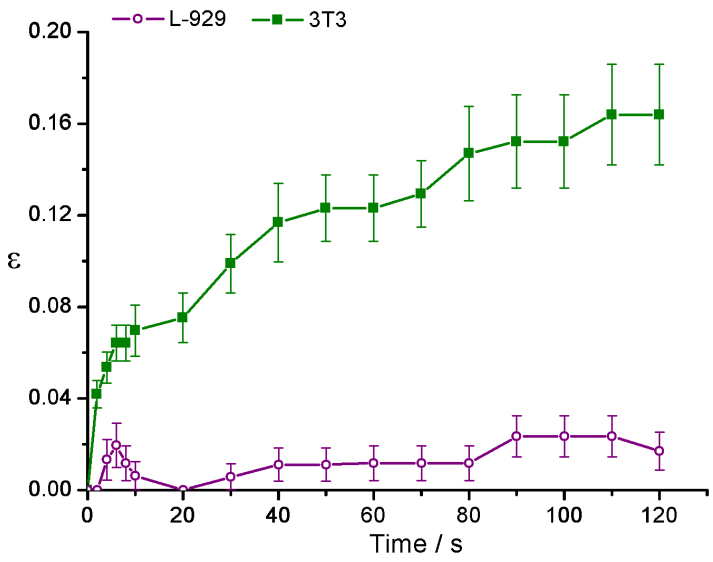

Figure 4.12: Mean value of the stretching of L-929 and 3T3 fibroblast cells.

4.3.2 Analysis of fibroblast cells

For further validation of our newly developed device, the response to electric deformation was also analyzed by means of the dielectrophoretic stretcher in another pair of adherently growing, nonmalignant and malignant cell lines. Using the same set-up 3T3 and L-929 fibroblast cell lines were stretched and their respective elongation was measured. It is known that these two fibroblast cell lines show different tumorigenic behavior - 3T3 cells can be considered nonmalignant while the L-929 are malignant cells [23–25]. They showed different reactions when they were stretched by the electric field (Fig. 4.12). However, by averaging over all data from measured cells, valuable information is lost which is possible to retrieve from the analysis of the individual cells. Therefore, a cell by cell assessment was chosen to elucidate the particular behavior of the L-929 cells in the electric field. In Figures 4.13 and 4.14 the reactions of eight single cells per cell type are depicted.
In contrast with 3T3 cells that undergo a continuous deformation over the observation time, L-929 cells show a reaction to the electric force that is composed of an initial lag phase without any visible reaction followed by a step deformation after varying times and of different durations. This feature allows to clearly distinguish between the two fibroblast types. The deformation of the L-929 cells during the time of exposure to the electric field is always smaller than that of the 3T3 cells. The mean values of the deformation of the two cell lines shown in Figure 4.12

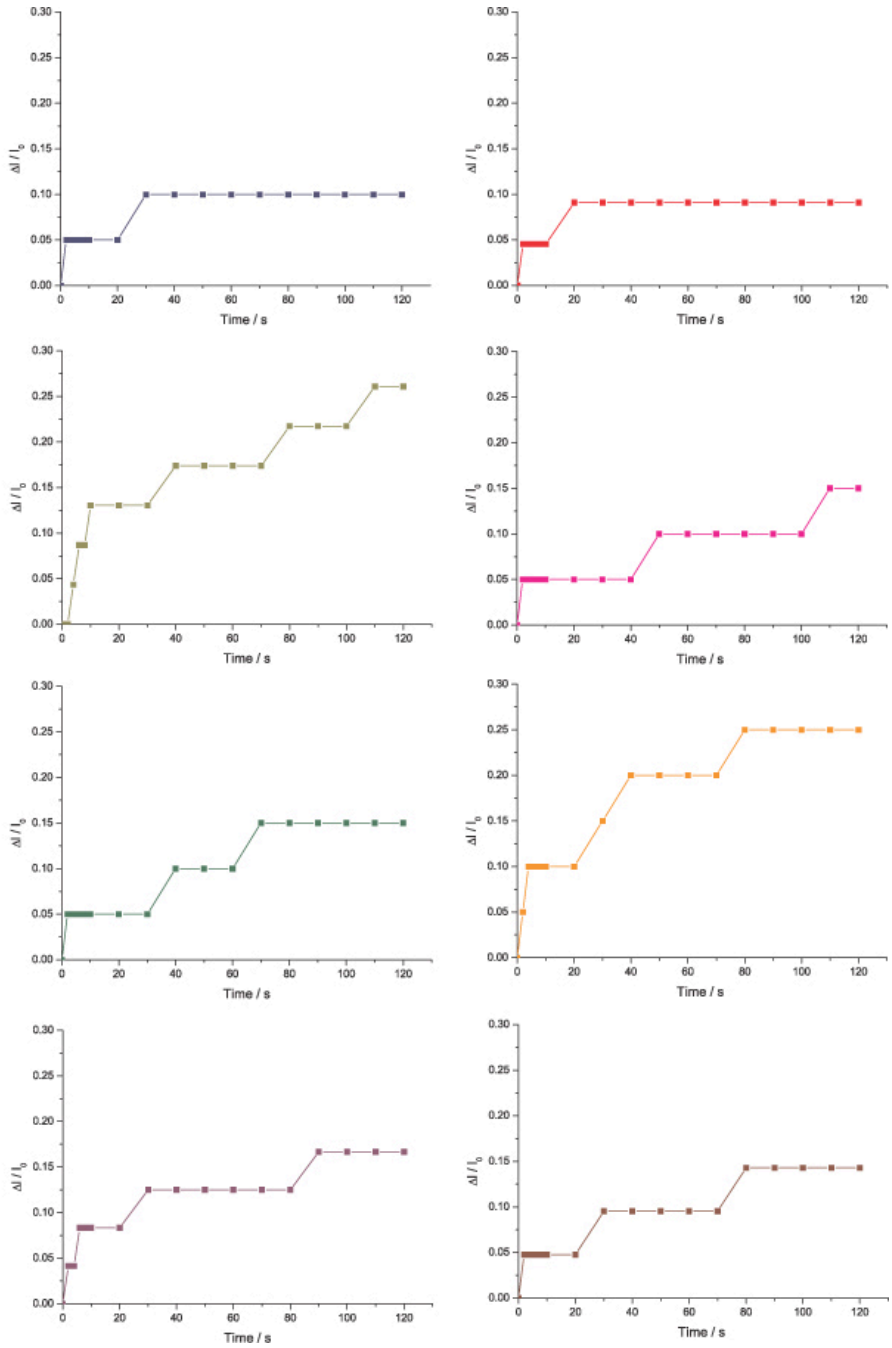

Figure 4.13: Stretching of single 3T3 fibroblast cells.

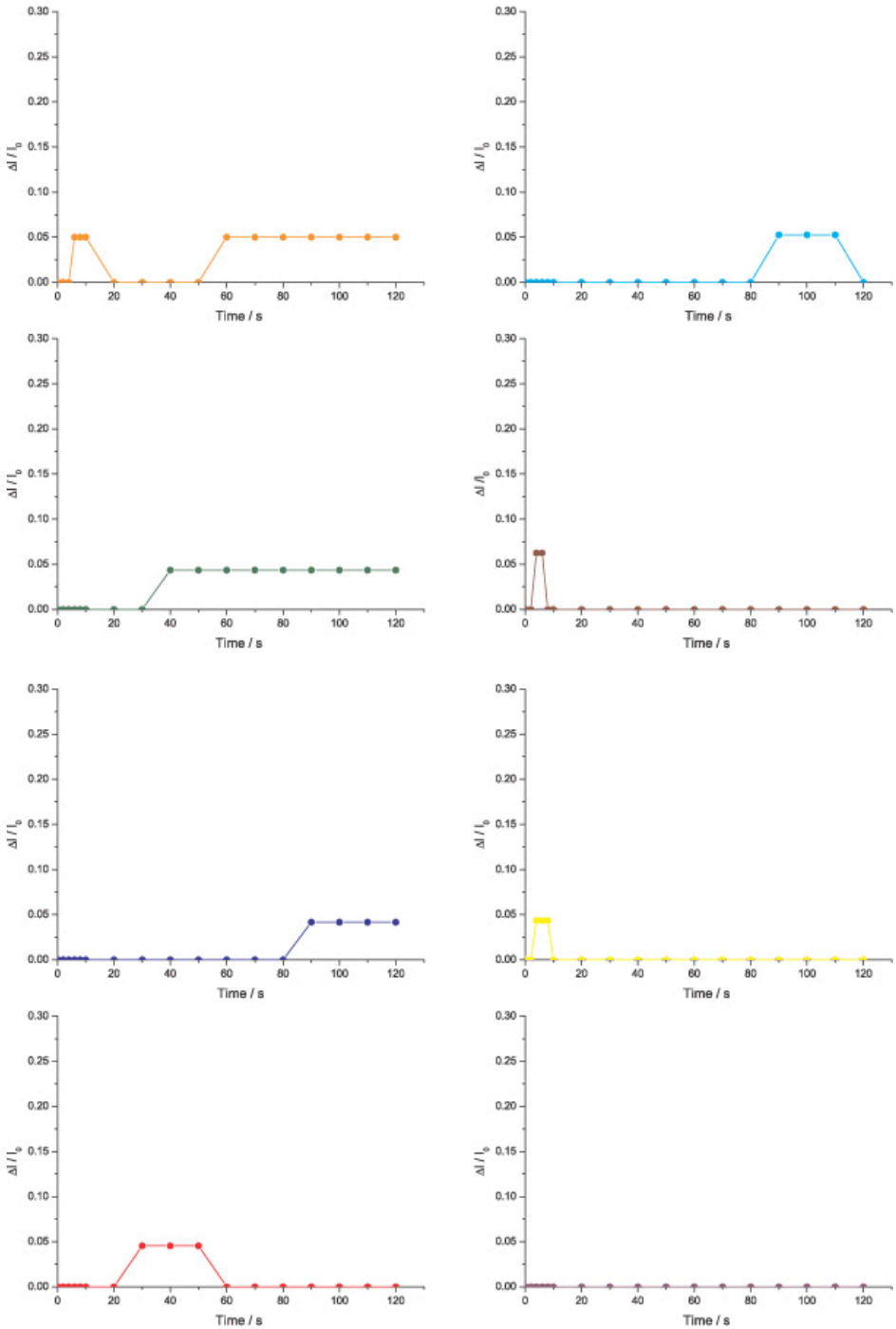

Figure 4.14: Stretching of single L-929 fibroblast cells. The cells do not deform continuously over the time, but show a behavior in the electric field that is clearly different from that of 3T3 fibroblasts (see Fig. 4.13).

provide a helpful overview of the cellular stiffness. The L-929 cells turned out to be stiffer than the 3T3 cells. Again, as in the case of the MCF cell lines detailed above, the nonmalignant cells are considerably softer than the malignant cells when they are deformed by an electric field. These experiments are an additional confirmation that our technique can be used to characterize different cell lines for distinguishing between cancerous cells and their nonmalignant counterparts.

4.3.3 Mesenchymal cells

As a third cellular test system of adherent cells, we analyzed mesenchymal cells with our technique. These cells were directly obtained from biopsy samples from human knee tissue. This tissue is assumed to contain stem cells while the majority of cells is of fibroblastic type. The idea, therefore, was to investigate whether the stem cells could be identified by potential differences in their stretching response as compared to the fibroblasts and other cell types. No significant electric elongation was visible with applied voltages of up to 6 V. Further variations in the electric force exerted only led to membrane breakdown and subsequent bleb formation. Later analysis of the samples by conventional techniques indicated that they actually did not contain stem cells.

4.4 Stretching of suspension cell lines

In the following chapter we turn from employing the dielectrophoretic stretcher for characterization of adherent cells to that of suspension cell lines. Here, our main aim was to investigate the influence aging culture medium has on the mechanical properties of the cells. The standard cell culture procedure is to split cells in culture every three days, i.e., the cells are usually supplied with fresh medium in this interval. For our analysis, we compared cultivation durations without splitting for up to five days. In order to investigate the influence of the cultivation duration on the viscoelasticity of the cells, we dielectrophoretically stretched samples of cells for 90 s on the days two to five. Since suspension cells exhibited a greater electric sensitivity in comparison with adherent cell lines, the voltage applied in these experiments was 4 V instead of 6 V. Three different cell lines served as model systems for the examination of the response to the dielectrophoretic deformation: HL-60, U-937 and Jurkat cells.

4.4.1 Analysis of HL-60 model system

In order to gain a better insight into the influence of the cultivation duration on the viscoelasticity of the cells, we analyzed the dielectrophoretic stretching on a single-cell level as a measure of the mechanical properties of HL-60 cells. The experiments showed that the cellular stiffness effectively depends on the cultivation duration: The longer the cells were cultivated without splitting, the softer they appeared in the electric field (Fig. 4.15). The next step was to prove that the dif-

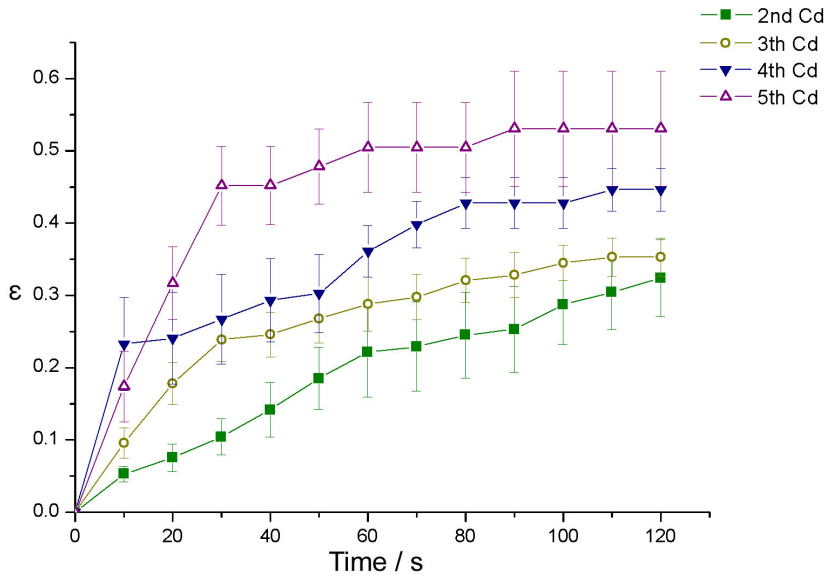

Figure 4.15: Deformation vs. time of HL-60 cells at different cultivation days. The concomitant loss in cellular rigidity is clearly visible.

ferences in the stretching response were due to changes in the medium occurring over time. For this approach, we transferred the "used-up" medium of cells that had been in culture for four days to "fresh" cells that had been cultivated for only one day. In a separate second assay, four-days-old cells were supplied with fresh medium. In both cases, the stretching was measured 24 h later. We found that the five-days-old cells in fresh medium were stiffer than control cells that had been without fresh medium for five days (Fig. 4.16-B). Conversely, two-days-old cells in "old" medium appeared softer to the electric deformation than control cells in two-days-old medium (Fig. 4.16-A). The purpose of medium change in cell culture is to maintain the correct pH value and to replenish nutrients. Therefore, these two factors were separately investigated next to determine which of them causes the change in the cellular stiffness of HL-60 cells.

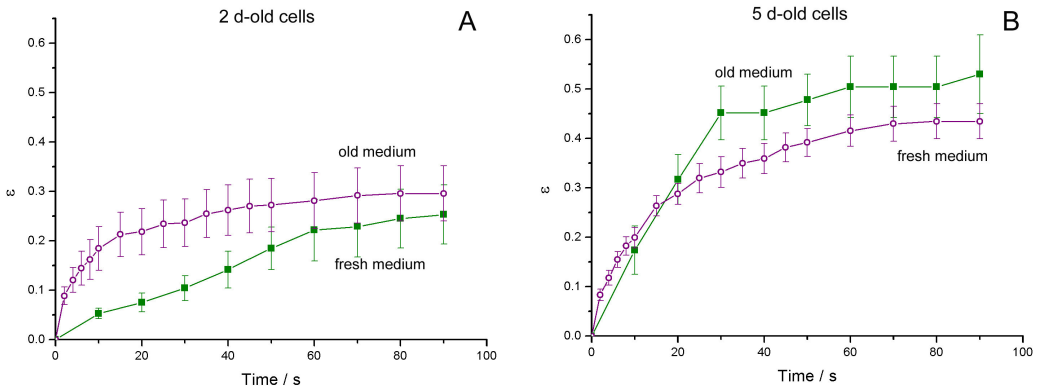

Figure 4.16: Change in the stretching behavior of HL-60 cells in the course of several cultivation days is due to effects of altering medium composition. A. Experimental data of cells stretched on the second cultivation day. These two-days-old cells were either grown in fresh (2d-old) medium or in five-days-old (i.e. depleted) medium. The latter exhibit a clearly reduced cellular rigidity, in particular in the first 40 s of the stretching. B. Cell stretching on the fifth cultivation day. These cells had either been exposed to the same medium for five days without exchange ("old medium") or they had been supplied with fresh medium 24 h before the measurements ("fresh medium"). A tendency towards an increased stiffness is visible in the experiments employing the cells supplied with fresh medium. This is interpreted as a recovery from the effect of old medium.

Influence of the pH value. The pH value of the cell culture medium was measured daily for five cultivation days. The values decreased from 7.6 to 7.1 (Fig. 4.17). This gradual shift in the pH value was simulated in fresh medium by adding hydrochloric acid (HCl). Thus, fresh medium was obtained with the same pH value as that of the five-days-old medium (7.1). In this case, one-day-old and four-days-old cells were cultivated for 24 h. Subsequently, they were stretched and the results compared with the corresponding data shown in Figure 4.16. From these experiments, the two following conclusions could be drawn: as depicted in Figure 4.18-A, two-days-old cells in fresh medium with the pH value of five-days-old medium were stiffer than two-days-old cells that had been cultivated for 24 h in five-days-old medium (with the corresponding pH value of 7.1). Conversely, five-days-old cells in fresh medium (pH 7.6) and in fresh medium with the pH value of five-days-old medium (pH 7.1) showed comparable results, although in both cases the cells were in fresh medium (Fig. 4.18-B). These results show that, in the range investigated, the pH value was not the factor responsible for variations of cellular rigidity. Instead, the rigidity was apparently influenced primarily by whether the medium was fresh or not, irrespective of its pH value. Therefore, other parameters of the medium that change over time had to be tested next.

Figure 4.17: The pH value of cell culture medium measured during cultivation for five days without intermittent cell splitting. A continuous acidification becomes apparent.

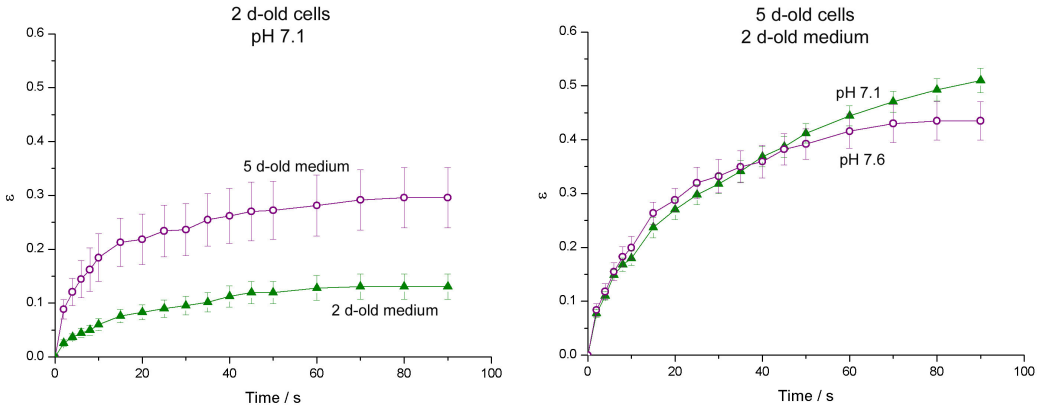

Figure 4.18: A. HL-60 cells on the second cultivation day in either five-days-old medium (open circles) or in pH-reduced fresh medium (full triangles) respectively. The two media had the same pH value, but different effects on the cellular stiffness. The fresh medium was the decisive factor in the HL-60 cell rigidity, as shown in B. Here, the two five-days-old HL-60 populations exhibited the same dielectrophoretic deformation, although the pH values of the media were different. Both cell samples were cultivated for 24 hours in fresh medium.

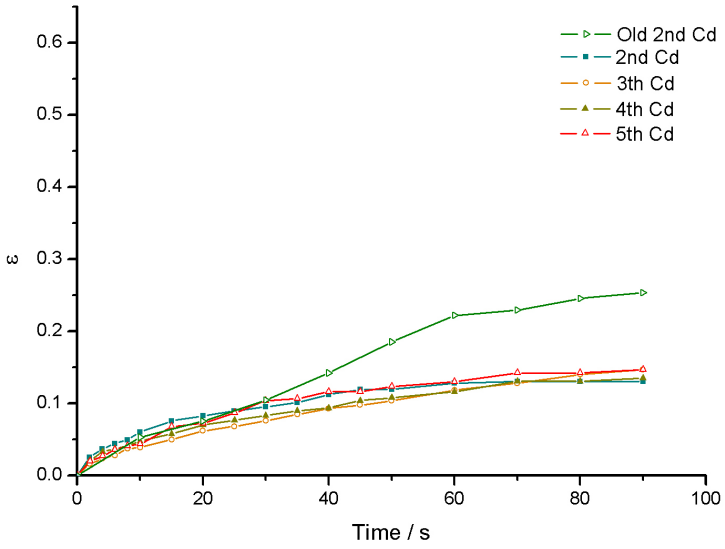

Figure 4.19: The continuous fresh medium supply leads to constant cellular mechanical properties. For comparison, the loss in the rigidity of the HL-60 cells after cultivation for two days without medium exchange is also shown (Old 2nd Cd). Error bars omitted for clarity.

Influence of nutrient depletion. The next step was to investigate whether the differences in the stretching behavior of HL-60 cells were caused by nutrient depletion of the medium. For this purpose, we daily removed the old medium on five consecutive cultivation days and supplied the cells with fresh medium. This was achieved using microtiter plates and well-inserts with 1 μm pore size. Every 24 h, a sample of the cells was stretched. No difference was observed in the resulting deformation curves (Fig. 4.19). This in turn strongly suggests that the change in viscoelasticity of the HL-60 cells in our experiments is primarily determined by nutrient depletion.
We now corroborate these findings in HL-60 cells by extending our analysis to other suspension cell lines.

4.4.2 Analysis of further suspension cell lines

In order to strengthen our analysis of the change of cellular properties due to aging medium, we carried out stretching experiments with two other cell lines: U937 and Jurkat cells. Again we investigated the influence of the cultivation day on the viscoelasticity of the cells. Figure 4.20 shows the results of the stretching of these cell lines. It is clearly visible that the aging medium has not the same effect on these cell types as on HL-60 cells. The mechanical properties of the

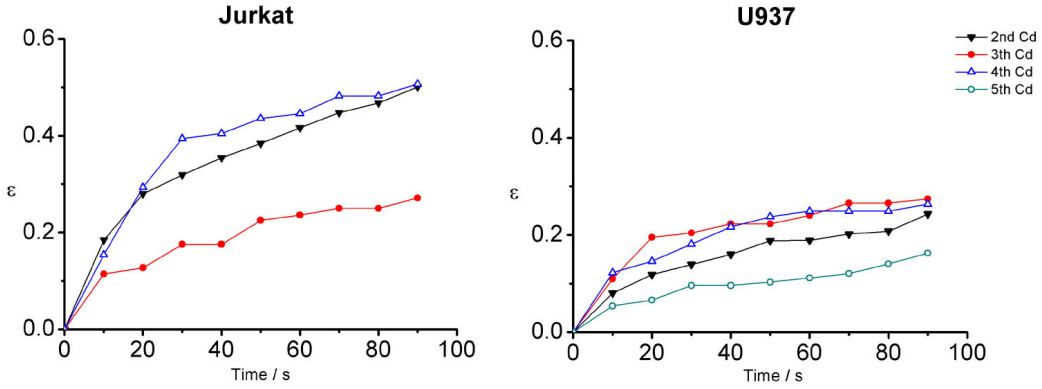

Figure 4.20: Deformation response for U937 and Jurkat cells. It is clearly visible that the aging medium has not the same effect on these cell types as on HL-60 cells.

Jurkat cells fluctuate between maximal and minimal deformation values over the time. It was not possible to stretch these cells on the fifth cultivation day because of breakdown of their cellular membrane. Probably this was due to weakening of the cells caused by aged medium. U937 cells presented only little variation of their mechanical properties over the five cultivation days (see Fig. 4.20). The greatest difference occurred on the third and on the fifth cultivation day.

These additional experiments show that the influence of the aging medium on cells also depends on the cell type. HL-60 cells are leukocytes, Jurkat cells are lymphocytes and U937 are cells of lymphoid tissue. In conclusion, the results presented in this paragraph underline that extensive care has to be taken in cell culture in order to guarantee reproducible outcomes. The important lesson to be learned from this section is, that it is significant to maintain absolutely constant conditions in cell culture in order to obtain reproducible and reliable data.

4.5 Analysis of chip heating

The application of electric fields as described implies that Ohm's heating is induced in the fluid and in the cells and that the temperature might markedly rise in a small sample volume. An appropriate evaluation is very important for experiments with biological systems, because a temperature rise could lead, for example, to denaturation of material components or to the induction of heat-related stress proteins, like HSP and other chaperons.

In order to estimate the increase in temperature ΔT in our system caused by the electric field, we employed infrared (IR) thermography to analyze the temperature distribution on the chip. In our view, this choice is more appropriate than using, for example, a resistance temperature sensor. Its introduction into the fluid in the

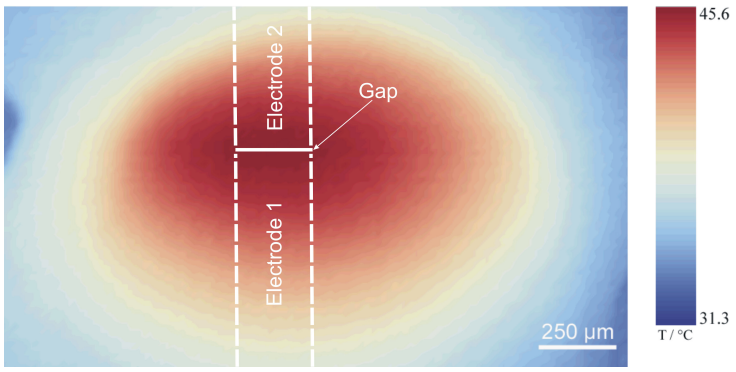

Figure 4.21: Top view of an infrared photograph. It was obtained for a 20 μm gap width. The electric conductivity of the buffer was 1.4 S / m.

silicone trough could itself influence the measurements. We filled the trough on the chip with buffer and carried out the temperature measurements as described in chapter 3. Multiple measurements were taken, systematically varying the values of the following parameters: the voltage, the gap width between the electrodes and the buffer conductivity.

Figure 4.21 shows a typical image as obtained from the entire chip area, which measures less than one square centimeter. The electrode edges were depicted by the dashed lines. As expected, the temperature reaches its maximum value between the microelectrodes. The maximum temperature value T_{max} of each thermal map was extracted. Then the resulting data were fitted to

$$T = T_0 + \Delta T \qquad \text{with} \qquad \Delta T = k\sigma U^2 \tag{4.8}$$

where T_0 is the ambient temperature. k depends on the geometry and on the medium thermal conductivity. Through the fitting, the values of k for the two given geometries were derived :

- k_{20} = (0.65 $\pm$ 0.09) °C m / W
- k_{35} = (0.89 $\pm$ 0.09) °C m / W.

By means of these parameters values and using the eqn. 4.8, the temperature that has to be expected can be estimated for any given voltage and fluid electric conductivity. Concluding from the two k-values found, the increase in temperature in the 35 μm structure is clearly greater than that in the 20 μm structure under otherwise equal conditions. The reason is that the same amount of thermal energy fed into a smaller system is much better dissipated due to its high surface to volume

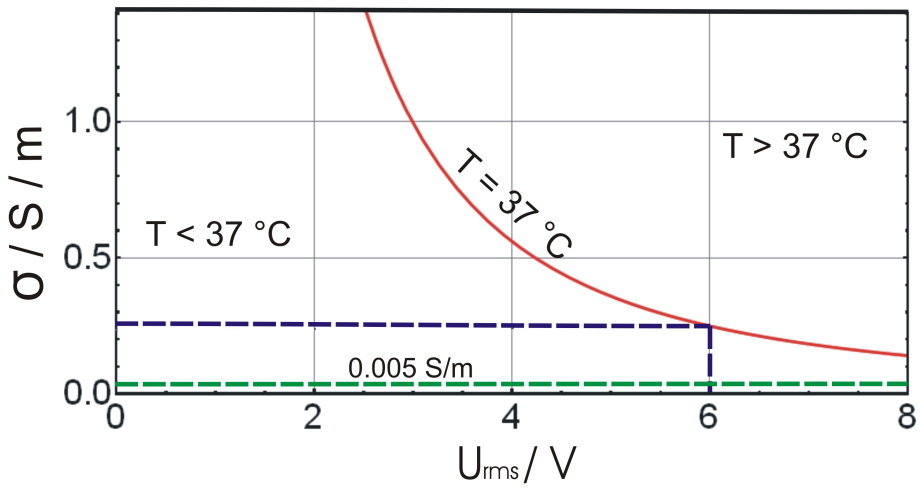

Figure 4.22: Plot of the isotherm of 37 °C for the case of the 20 μm gap width according to eqn. 4.8. The dashed lines indicate the buffer electric conductivity used in our experiments (0.005 S / m, green) and the voltage of 6 V that was mainly employed (blue). Our observations of cell stretching were made far in an uncritical region of T $<$ 37 °C.

ratio. This relationship is described by Fourier's law of heat conduction:

$$Q = \lambda \cdot \frac{S}{d} \cdot \Delta T \tag{4.9}$$

where λ denotes the thermal conductivity. At a distance d from the surface S, a temperature rise of ΔT relative to the environment occurs inside the heated volume. Thus, reducing the dimensions of the system results in a lower temperature increment. This is an additional argument for our choice of a gap width of 20 μm. Employing the characteristic k value, the eq. 4.8 was used to plot $\sigma(U)$ for the 20 μm gap and for T = 37 °C constant (Fig. 4.22). This isotherm is depicted in the graph. It divides the plane into two temperature areas: one of $T <$ 37 °C, at low voltages and electric conductivities and vice versa. The first of these two covers a suitable parameter space when working with live cells. In order to remain within the safe temperature zone based on this calculation, 6 V, i.e. the voltage used during the stretching experiments, allows for a maximum of the electric buffer conductivity σ = 0.25 S / m, marked in the graph by the blue dashed line. This value is 45-fold higher than that of the buffer that we used in our experiments. The graph can also be interpreted for a given electric conductivity of 0.0055 S/m (marked in the graph by a green dashed line). In this case, the voltage that can safely be applied without probable thermal damage to the cells far exceeds that used in our experiments. For instance, much higher electric field

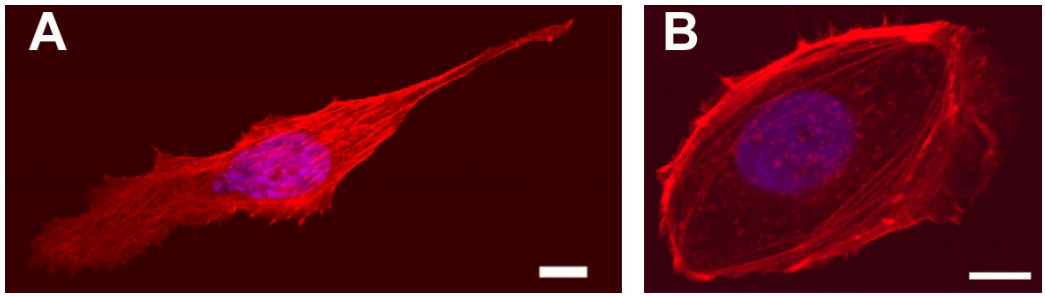

Figure 4.23: Staining of actin and cell nucleus of MCF-10A (A) and MCF-7 (B) by means of phalloidin (red) and DAPI (magenta) respectively. The scale bar is 10 μm.

strengths could be applied without cell damage. So, our newly developed dielectrophoretic stretcher works in an ample parameter space that is safe to use also with other cell lines.
The measurements of the temperature distribution on the surface of our chip and the isotherms calculation showed that in the voltage and the buffer electric conductivity range that we used, our system produces only a small temperature increment. The parameter set selected ensures that the heating is far from harmful to mammalian cells, i.e. beyond the 37 °C limit, and, therefore, negligible.

4.6 Visualization of cytoskeleton structures during stretching

The final section of this chapter focuses on the visualization of cytoskeletal filaments during the stretching in the electric field.

Convenient methods were developed to stain cytoskeletal structures in fixed and living cultured cells. We employed different staining procedures for the actin filaments and the microtubules of MCF-10A and MCF-7 cells. In Figure 4.23 the results of the fluorescence staining of cellular nucleus and actin filaments are seen for MCF-10A cells, on the left, and MCF-7 cells, on the right. According to the corresponding protocols, the cells were fixed and then stained using Phalloidin for the actin filaments and DAPI for the nucleus. As is visible in the figure, the F-actin filaments in both cell types extend through the whole cell.

In order to visualize microtubules, we labelled the cell lines by transfecting them with α-tubulin-GFP-construct. Together with β-tubulin, α-tubulin is the subunit that forms tubulin dimers, the basic structural units of microtubules.
GFP is a fluorescent protein tag, that can be linked to almost any protein including cytoskeletal proteins. It serves as a visual reporter of dynamic events occurring in living cells. On the contrary, labeling cytoskeleton with fluorophores such as

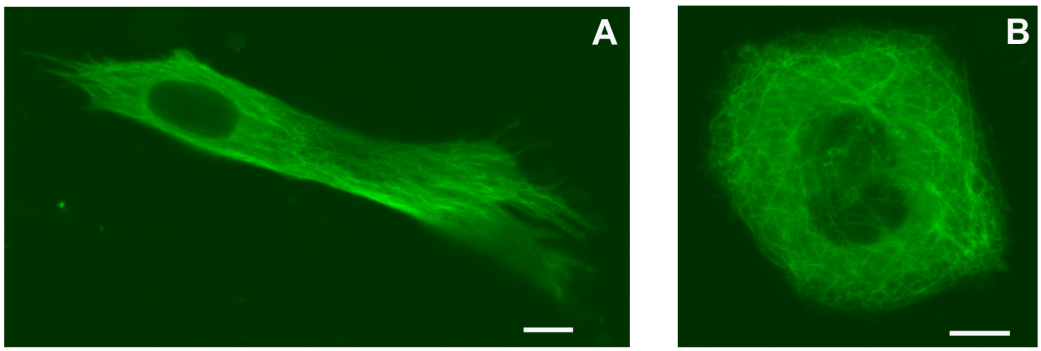

Figure 4.24: Visualization of microtubules of GFP-transfected MCF-10A (A) and MCF-7 (B). The scale bar is 10 μm.

rhodamine needs fixed cells, i.e. dead cells. Cells transfected with GFP were previously reported to display viscoelastic properties identical to nontransfected cells [59].
Five days after the transfection, an optimal visualization of the tagged protein was obtained. In Figure 4.24 GFP-transfected MCF-10A and MCF-7 cells are shown. The images were collected using a confocal laser scanning microscope (clsm). The differences in microtubule distribution in the two cell types is clearly visible: in the MCF-7 cells microtubules were spooled around the cellular nucleus, whereas in the MCF-10A they stretched through the whole extent of the cell as they were positioned parallel to each other.
We stretched the fluorescent cells while recording the experiments. For the experiments, we used a high resolution microscope objective (100 X water immersion objective).
Figure 4.25 shows the microtubules of a transfected MCF-7 cell, which were visible during the stretching by the electric field. In comparison with the microtubules organization of the adherent MCF-7 cell showed in Figure 4.24-B, the microtubules of the MCF-7 cell in suspension appeared as an irregular filamentous network rearranged in the volume.

MCF-10A cells were also stretched in the electric field after being transfected. In this case, it was not possible to recognize the microtubules as a group of individual filaments as in the case of the MCF-7 cell. During the stretching of MCF-10A cells the interior of the cell was visible as a homogeneous fluorescent volume. It could depend (I) on the different microtubules organization of the MCF-10A cells in comparison with MCF-7 cells and (II) on nonoptimal observation condition.
(I) Referring to Figure 4.24, we suppose that after cell trypsinization, the parallel organization that the microtubules have in MCF-10A cells can not take place and the microtubules collect them in a compact mass. On the contrary, the microtubules of the MCF-7 probably maintain a spool form.

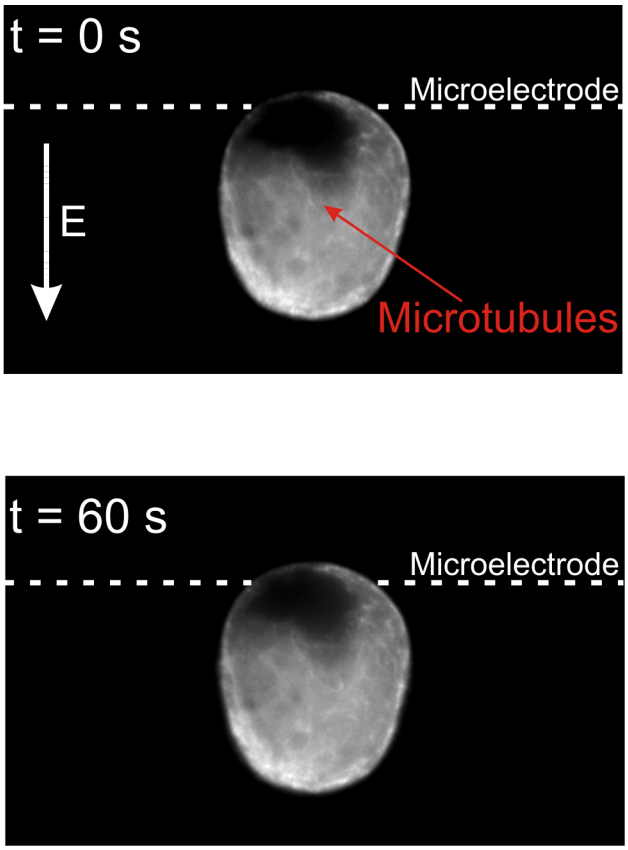

Figure 4.25: Visualization of GFP-transfected microtubules in a MCF-7 cell during stretching in the electric field E, the direction of which is depicted in the figure. The microstructures are already visible at the beginning of the experiment. After 60 s it is still possible to observe the filaments.

(II) The images of Figure 4.24 were collected using a confocal microscope, which has the advantage to collect light from a narrower z-section (along the optical axis) in comparison with a convectional microscope. This is achieved by excluding most of the light from the specimen apart from the microscope's focal plane, obtaining a better contrast. On the contrary, the convectional microscope, like the one we used, detects both focused and unfocused image components. This could be the explanation for the fluorescent haze visible in the interior of MCF-10A cell and that probably made microtubules invisible. It was not possible to carry out the stretching experiments using the confocal microscope, because the set-up of our chip was not suitable for inverted microscope.

After 60 s that the cell was stretched in the electric field, no modifications of the distribution of the microtubules were visible. We assume, that both the polarization of the cell interior due to the electric field and the mechanical deformation

did not cause large changes in the structural organization of the analyzed cell, when it is stretched up to 10% of its size. In the light of this result, our new technique results to be noninvasive, preserving the integrity of the cellular structures.

The result obtained with these experiments shows that combining GFP-transfection with the dielectrophoretic stretching various molecular events in living cells can be visualized. This allows the study, for instance, the effects of drugs on the structure of the cytoskeleton as well as on other cellular components. Such studies can be helpful to verify the effectiveness of specific treatments.
The dielectrophoretic stretcher can be considered a technique compatible with optical investigation for studying the behavior of a cell's internal components during mechanical deformation, without damaging the analyzed cell.

4.7 Integration into a microsystem

The last important step of our work described in this thesis is the integration of the dielectrophoretic stretcher into a microfluidic system (Fig. 4.26).
The microfluidic device shown in Figure 4.26-A was manufactured as follows:

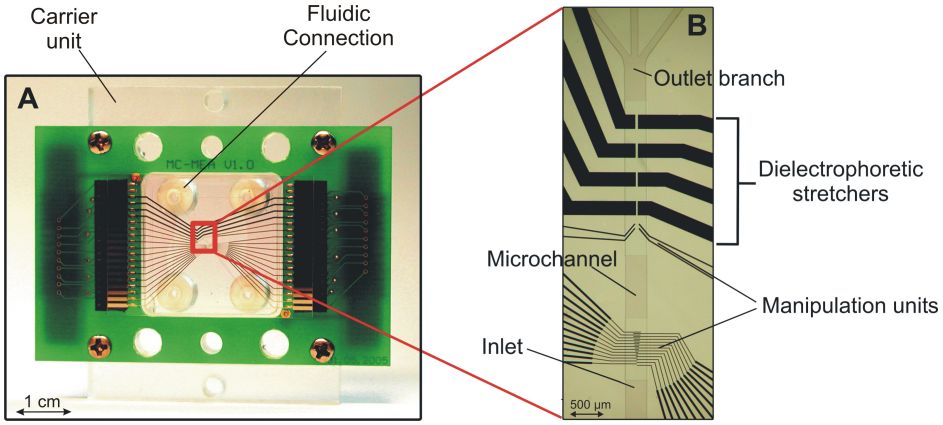

Figure 4.26: Integration of the dielectrophoretic stretcher into a microfluidic device. A. The microchip basically consists of a glass plate equipped with microelectrodes (visible in the figure). The glass plate adheres to a polymer structure that forms the channel. The microelectrodes are connected with the generator via the green circuit board. B. Integrated dielectrophoretic stretcher elements. Four electrode pairs with different gap widths were processed. Other manipulation units are also visible in the figure. The triple branched outlet is ideal for a sorting operation.

The electrodes were processed on a glass slide by photolitography. The channel was moulded on a polydimethylsiloxane (PDMS) slide, which is a biocompat-

ible material. These two slides were sandwiched and mounted on a Polymethylmethacrylate (PMMA) carrier in order to obtain a stable structure. The PMMA carrier also serves as support for the fluidic connection, e.g for standard HPLC-tubes, and for the green circuit board, which is the interface between the external generator and the microelectrodes.
Figure 4.26-B shows an enlarged view of the flow channel with the electrode structures of the dielectrophoretic stretcher. The electrode arrangement and the channel geometry were designed with the help of a CAD software (AutoCAD, Autodesk, Inc.). Different electrode gap widths, e.g. for different cell types, were processed in the chip. The electrode structures positioned between the inlet and the stretchers are dielectrophoretic units useful for hydrodynamic pumping, aligning and positioning of cells. The triple branched microfluid channel provides three outlets. By positioning electrode pairs at the branching point, it is possible to sort cells by deflecting them towards the outlet of interest. Into the microsystem described here, which was the first one to be technically realized, the outgoing deflector electrode pairs were not processed, because of a communication problem. Lacking the sorting unit, the device did not allow to carry out experiments. The design was suitable for stretching in a microfluidic device, but it needed technical correction in the processing procedure to permit an optimal combination of the novel stretcher with dielectrophoretic manipulation units for aligning, sorting and positioning of cells. Because of the time required to provide a new processed structure, it was not possible for us to make the correction.

The realization of this microsystem device shows that the entire cell processing lines can be established in a chip format.
Nowadays substantial progress has been achieved in processing microelectrodes into microsystem. This allows the integration of the dielectrophoretic stretcher into a microfluidic device by using inexpensive methods.
The design optimization of chips like our stretcher with a simple set-up and a considerable throughput is the logical next step forward.

CHAPTER 5

Conclusions

Non-uniform electric fields applied to a cell suspension give rise to polarization effects of the charges in the cells that induce translational motion of these cells. This phenomenon is called dielectrophoresis and can be exploited to guide cells towards the region of interest. Related to this effect is the dielectrophoretic elongation of cells between two microelectrodes which generate the electric field.
By using the dielectrophoretic force induced on the cells by the electric field, we developed a technique to characterize the mechanical properties of different cell types and to distinguish them according to their stiffness. The main results obtained by the experiments that we carried out and described in this thesis are highlighted in the following. They can be summarized in four major points:

- by stretching a relatively small number of cells from two pairs of adherent cell lines, each with malignant-nonmalignant feature, reliable data were obtained that allowed unambiguous distinguishing between cancerous and noncancerous cells (section 4.3)

- by stretching suspension cells cultivated for different durations, it was shown

that a relation between the cellular stiffness and the aging of the culture medium existed (section 4.4)

- the analysis of the chip heating by using infrared thermography proved the suitability of this technique for working with biological cells (section 4.5)
- the visualization of the microtubules of the cells during the stretching in the electric field demonstrated that the dielectrophoretic stretcher is compatible with optical investigation of the effect of the mechanical deformation on the internal structures of the cell (section 4.6)
- the integration of the dielectrophoretic stretcher into a microfluidic system.

In the following, the main conclusions from each of these points will be summed up

In **section 4.3** we describe the application of the dielectrophoretic stretcher to four cell lines of two different types. We analyzed a pair of human cell lines, one of cancerous origin (MCF-7) and the other one derived from related non-cancerous tissue (MCF-10A), as well as a pair of animal cell lines, one of malignant origin (L-929) and the other one of nonmalignant origin (3T3). Based on a relatively small number of cells, reliable data were obtained that allowed unambiguous distinguishing cells of each pair. In both cases, nonmalignant cells turned out to be softer than their malignant counterparts. A detailed analysis of the dielectric properties of the human cells using dielectrophoretic spectroscopy showed that the differences in the stretching response are not the result of differences of the polarizability of the two cell types. Instead, the stretching response appears to be mainly determined by cell-specific mechanical properties. In order to deduce which parts of the cytoskeleton of the two cell types are mainly responsible for the different stretching behavior, two cytoskeleton-specific toxins were applied to the human cells during the measurements. Addition of latrunculin A, which inhibits actin polymerization, leads to comparable relative changes of the deformation response of both cell types. The use of colchicine, which blocks microtubule polymerization, softened both cell types, so that they exhibited approximately identical absolute strain values. This indicates that differences of the microtubule structures of the two types are the cause for their different response to dielectrophoretic stretching.

Section 4.4 focuses on investigating the influence of aging culture medium on the mechanical properties of suspension cells. Three different cell lines served as model systems for the examination of the response to the electric deformation:

HL-60, U-937 and Jurkat cells. Comparing the response to stretching after cultivation durations without splitting the cells of up to five days, we obtained data that clearly showed that the cellular stiffness effectively depends on the cultivation duration. The pH value and the culture medium depletion were identified as potential factors responsible for the different deformation over time. A detailed analysis of the influence of the pH value on the mechanical properties of HL-60 cells was carried out. These results showed that the rigidity was primarily influenced by whether the medium was fresh or not, irrespective of its pH value. Thus, in the investigated range, the pH value has not any influence on the cellular rigidity. In order to verify this result, we analyzed the response to stretching of cells, which were continuously supplied with fresh culture medium for the entire cultivation duration. The results of this last experiment strongly suggest that the changes in the stiffness of the HL-60 cells in our experiments were primarily attributable to nutrient depletion.

Section 4.5 describes the analysis of Ohm's heating induced in the sample volume and the possible temperature rise in the small volume of sample. In order to estimate the increase in temperature ΔT in our system caused by the electric field, we employed infrared (IR) thermography to analyze the temperature distribution on the chip. Multiple measurements were taken, systematically varying the values of the following three parameters: the voltage, the gap width between the electrodes and the buffer conductivity. The measurements of the temperature distribution on the surface of our chip and the subsequent isotherms calculation showed that our system produces only a neglegible temperature increment in the voltage and buffer electric conductivity range chosen for the stretching experiments. The parameter set selected for our experiments ensures that the heating is far from being harmful to mammalian cells, i.e. it is well within the 37 °C limit.

The **section 4.6** focuses on visualizing cytoskeleton structures during stretching by the electric field. We used fluorescent labeling of the cells by GFP transfection. Then we applied our dielectrophoretic stretcher to the cells as detailed before, and this allowed the visualization of the microtubules of the cells. No variations of the structures were observed during the stretching. This result demonstrates the noninvasiveness of our technique. By using GFP to visualize various molecular events in living cells, the dielectrophoretic stretcher can be considered a suitable technique for allowing simultaneous visualization for studying the behavior of a cell's cytoskeleton during mechanical deformation, without causing damage to the cells.

The final **section 4.7** describes the integration of the dielectrophoretic stretcher into a microfluidic system. Different electrode gap widths, e.g. for different cell

types, were processed in the chip. The design of the structure was suitable for stretching analysis in a microfluidic device. In the first system, which was technically realized, the outgoing deflector electrodes were not processed. Lacking the sorting unit, the device did not allow to carry out experiments. It was not possible for us to process a new chip within an acceptable period.

The experimental results described in this thesis clearly demonstrate the enormous potential of the novel dielectrophoretic stretcher. It was proven to be a reliable method to unambiguously distinguish between cells according to their different mechanical properties. These results underline that our newly developed dielectrophoretic stretcher can be promising for biotechnology and biomedical applications.

CHAPTER 6

Outlook

The results presented in this thesis indicate considerable potential for future developments of the project. The next steps to be undertaken can be categorized under biological (B) and technical (T) aspects.

The **biological issues** comprise the following subtopics which are explained in more detail in the next paragraphs:

B1. validation of the method to establish its suitability for diagnostic purposes

B2. additional studies of cellular mechanical properties by means of a ramp stress and a pulse train

B3. the analysis of intermediate filaments in order to complete the cytoskeletal structures analysis

To B1) Method validation by using primary cells. This first subtopic concerns the validation of the method of distinguishing between malignant and non-

malignant primary cells.
Throughout this investigation, we worked with cell lines. The reason for this choice was that they are easily available and can be grown in cell culture for extended periods of time with very little effort. In contrast, primary cells, i.e. cells that are taken directly from living tissue (e.g. biopsy material), are only capable of not more than one or two divisions in vitro at best. In addition, they are difficult to obtain, since the procedure of their extraction is subject to considerable legal restrictions. However, primary cells represent a closer approximation to the in vivo situation than cell lines. Thus, we see the validation of our method by analyzing primary cells as an important step for establishing its suitability for successfully identifying cells. This could for example be accomplished by characterizing cells obtained from a biopsy sample according to their mechanical properties and then by comparing the outcome of the stretcher measurements with the results of disease (e.g. cancer) specific stainings.

To B2) Mechanical properties of cells. One part of this thesis is formed by results of stress-strain experiments, carried out to characterize the mechanical properties of the cytoskeleton. In this case, the stress applied on the cells was a single voltage step. Additional information on the mechanical properties of cells can be obtained from (I) stress-strain experiments by applying a ramp stress instead of a step stress and (II) the application of a pulse train, each pulse of which is of constant voltage and short duration. The experiment (I) yields information about the strength of the material. From it, it is possible to analyze the elastic regime of the cells and the transition to the plastic regime. Furthermore, the result can provide an approximate value of the Young modulus.
By applying a pulse train (II), the cells undergo continuous load and unload phases. The resulting data may give a deeper insight into the plastic regime, for example whereas the permanent deformation increases or remains constant over the observation time during the application of the pulse train.

To B3) Intermediate filaments. In this work, only the contributions of the actin filaments and of the microtubules to the dielectrophoretic deformation were analyzed. In future, the study of the behavior of the intermediate filaments during stretching in the electric field will be considered. Using depolarizing chemicals that are specific for intermediate filaments, e.g. acrylamide, might yield further interesting results.

Another direction of future work on our newly developed dielectrophoretic stretcher could be the **technical development** of the microsystem.
In paragraph 4.7, we presented the first stretcher integrated into a microfluidic

device. The future development of the device is intended to realize a microsystem device in which the entire cell analysis can be carried out automatically in a chip format: the cell suspension flows into the channel of the microdevice, the cells are individually trapped and deformed by the stretcher units and the deformation is analyzed. After the evaluation, each identified cell is transported towards its corresponding outlet. Thus, the cells can be sorted according to their cellular state (e.g. malignant, nonmalignant). For this purpose, we plan to develop:

T1. an algorithm for automatic deformation analysis

T2. a specific sorting unit

To T1) Algorithm development. The automated evaluation requires an algorithm that quickly and effectively analyzes the frames of the digital recording of the stretching experiments and subsequently controls the sorting unit. In order to develop the evaluation algorithm we intend to combine

- image processing tools for edge detection of a commercial software
- a procedure to evaluate the deformation

For the second point, we intend to take into consideration the procedure for evaluating the deformation amplitude described by Engelhardt and Sackmann [60]. The procedure will be customized for our purpose. A brief description of the expected operating mode will be sketched in the following. The stretching experiments are recorded by a digital camera and, by means of the commercial software, in each recorded frame the cell between the microelectrodes of the stretcher is detected. In the frame corresponding to t = 0 s, a line that includes the diameter of the cell is selected and maintained in each subsequent frame (Fig. 6.1). The deformation amplitude of the cell can then be determined by cross-correlating the intensity pattern of the line at t = 0 s with the intensity pattern of the line from each later image. This amplitude is finally compared with a threshold amplitude (characteristic of the analyzed cell type) and the cell is, thus, identified.

To T2) Sorting unit. The function of the sorting unit in a microfluidic system is to efficiently select the cells in order to allow a homogeneous cell collection for subsequent processing.
In a dielectrophoretic system the sorting unit is composed of microelectrodes (deflectors) that deflect the cells towards a selected outlet and the sorting of the analyzed particles occurs according to their different dielectric properties or their different size.
In our system, the cells have to be sorted according to their deformation degree

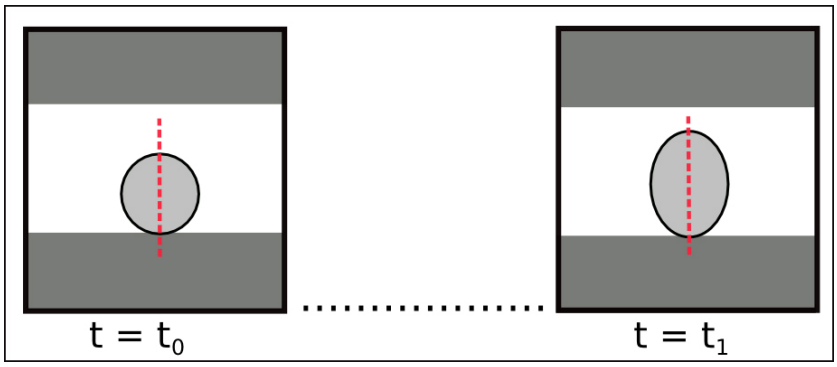

Figure 6.1: Representation of the image processing. From each frame, a pixel line will be extracted (red dashed line). By cross-correlating the intensity distribution along the line in each frame, the deformation amplitude will be obtained.

and, thus, the deflectors have to be controlled according to the evaluation procedure. An appropriate electrode configuration to realize the intended sorting unit was presented by [61] and is shown in Figure 6.2. This switch element is com-

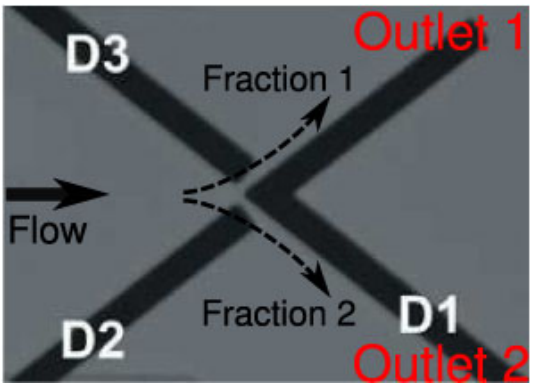

Figure 6.2: Electrode configuration used as switch element by Kirschbaum in [61]. This element consists of a central peak electrode (D1) and two deflection electrodes for sideward guiding (D2 and D3). For more details, see text. The width of the electrodes is 15 μm.

posed of a central peak electrode (D1) and two deflection electrodes for sideward guiding (D2 and D3). Depending on which of the three electrodes is inactive, an approaching cell is directed individually and very quickly to one of the three downstream outlets, from where it can be collected for subsequent purposes. Supposing that the cells, the deformation amplitude of wich exceeds the threshold value, have to be collected in outlet 1 (see Fig. 6.2), the evaluation procedure will send a signal to the generator to switch off the deflector D3 when the cell approaches the switch. Thus, the cells are properly separated. The efficiency of the procedure for sorting cells of different types will be verified by means of stains specific for the analyzed cells. We also intend to verify the harmlessness of the

system by cultivating the collected cells and observing their vitality.

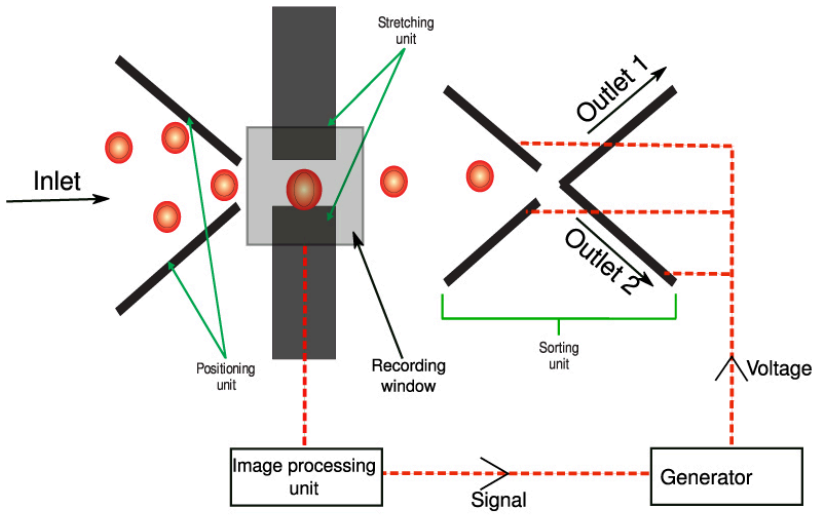

Figure 6.3: Schematic representation of the dielectrophoretic stretcher integrated into a chip for automatic process. For description see text.

Figure 6.3 shows a scheme of the entire microsystem for an automatic cell analysis. The positioning unit directs cells to the stretcher unit. When a cell is trapped by the electric field between the microelectrodes, the pump is switched off in order to avoid that other cells accumulate between the stretcher electrodes. The cell is then stretched and the experiment is recorded. The evaluation procedure identifies the cell and drives the generator to switch the corresponding deflector electrodes on or off. The pump is again switched on, so that the analyzed cell reaches the switch element and another cell is trapped by the stretcher electrodes.

According to our results (chapter 4), our dielectrophoretic stretcher can unambiguously distinguish between malignant and nonmalignant cells already after having analyzed 25 cells. The duration of the experiments described in this thesis was 60 s, but the results showed that the differences in deformation of the investigated cells already became visible after 10 s stretching. We intend to optimize the process in order to reduce the analysis time to 10 s. It the light of these considerations, the microsystem that will be developed in the future will be able to distinguish between malignant and nonmalignant cells in five minutes. The advantage of this system over time-consuming identification methods (staining procedures, for instance) makes of our integrated stretcher a highly promising tool.

Bibliography

[1] E. M. Darling, M. Topel, S. Zauscher, T. P. Vail, and F. Guilak, "Viscoelastic properties of human mesenchymally-derived stem cells and primary osteoblasts, chondrocytes, and adipocytes.," J Biomech, vol. 41, no. 2, pp. 454–464, 2008.

[2] C. Zhu, G. Bao, and N. Wang, "Cell mechanics: mechanical response, cell adhesion, and molecular deformation.," Annu Rev Biomed Eng, vol. 2, pp. 189–226, 2000.

[3] D. E. Ingber, "Mechanobiology and diseases of mechanotransduction.," Ann Med, vol. 35, no. 8, pp. 564–577, 2003.

[4] G. Bao and S. Suresh, "Cell and molecular mechanics of biological materials.," Nat Mater, vol. 2, pp. 715–725, Nov 2003.

[5] E. Rungger-Brändle and G. Gabbiani, "The role of cytoskeletal and cytocontractile elements in pathologic processes.," Am J Pathol, vol. 110, pp. 361–392, Mar 1983.

[6] S. Suresh, "Mechanical response of human red blood cells in health and dis-

ease: Some structure-property-function relationships," J. Mater. Res, vol. 21, pp. 1871–1877, 2006.

[7] S. Suresh, J. Spatz, J. P. Mills, A. Micoulet, M. Dao, C. T. Lim, M. Beil, and T. Seufferlein, "Connections between single-cell biomechanics and human disease states: gastrointestinal cancer and malaria.," Acta Biomater, vol. 1, pp. 15–30, Jan 2005.

[8] M. Radmacher, M. Fritz, C. M. Kacher, J. P. Cleveland, and P. K. Hansma, "Measuring the viscoelastic properties of human platelets with the atomic force microscope.," Biophys J, vol. 70, pp. 556–567, Jan 1996.

[9] K. J. V. Vliet, G. Bao, and S. Suresh, "The biomechanics toolbox: experimental approaches for living cells," Acta Materialia, vol. 51, pp. 5881–5905, 2003.

[10] R. M. Hochmuth, "Micropipette aspiration of living cells.," J Biomech, vol. 33, pp. 15–22, Jan 2000.

[11] E. A. Evans, "New membrane concept applied to the analysis of fluid shear- and micropipette-deformed red blood cells.," Biophys J, vol. 13, pp. 941–954, Sep 1973.

[12] M. Dao, C. T. Lim, and S. Suresh, "Mechanics of the human red blood cell deformed by optical tweezers," Journal of the Mechanics and Physics of Solids, vol. 51, pp. 2259–2280, 2003.

[13] O. Thoumine, A. Ott, O. Cardoso, and J. J. Meister, "Microplates: a new tool for manipulation and mechanical perturbation of individual cells.," J Biochem Biophys Methods, vol. 39, pp. 47–62, Feb 1999.

[14] O. Thoumine and A. Ott, "Time scale dependent viscoelastic and contractile regimes in fibroblasts probed by microplate manipulation.," J Cell Sci, vol. 110 (Pt 17), pp. 2109–2116, Sep 1997.

[15] J. Guck, R. Ananthakrishnan, H. Mahmood, T. J. Moon, C. C. Cunningham, and J. Kaes, "The optical stretcher: a novel laser tool to micromanipulate cells.," Biophys J, vol. 81, pp. 767–784, Aug 2001.

[16] J. Guck, S. Schinkinger, B. Lincoln, F. Wottawah, S. Ebert, M. Romeyke, D. Lenz, H. M. Erickson, R. Ananthakrishnan, D. Mitchell, J. Kaes, S. Ulvick, and C. Bilby, "Optical deformability as an inherent cell marker for testing malignant transformation and metastatic competence.," Biophys J, vol. 88, pp. 3689–3698, May 2005.

[17] H. A. Pohl, Dielectrophoresis. Cambridge University Press, 1978.

[18] J. Gimsa, P. Marszalek, U. Loewe, and T. Y. Tsong, "Dielectrophoresis and electrorotation of neurospora slime and murine myeloma cells.," Biophys J, vol. 60, pp. 749–760, Oct 1991.

[19] H. Engelhardt, H. Gaub, and E. Sackmann, "Viscoelastic properties of erythrocyte membranes in high-frequency electric fields," Nature, vol. 307,

pp. 378–380, 1984.

[20] F. F. Becker, X. B. Wang, Y. Huang, R. Pethig, J. Vykoukal, and P. R. Gascoyne, "Separation of human breast cancer cells from blood by differential dielectric affinity.," Proc Natl Acad Sci U S A, vol. 92, pp. 860–864, Jan 1995.

[21] T. Schnelle, T. Mueller, and G. Fuhr, "Dielectric single particle spectroscopy for measurement of dispersion.," Med Biol Eng Comput, vol. 37, pp. 264–271, Mar 1999.

[22] J. Gimsa, T. Mueller, T. Schnelle, and G. Fuhr, "Dielectric spectroscopy of single human erythrocytes at physiological ionic strength: dispersion of the cytoplasm.," Biophys J, vol. 71, pp. 495–506, Jul 1996.

[23] M. H. Makman, "Conditions leading to enhanced response to glucagon, epinephrine, or prostaglandins by adenylate cyclase of normal and malignant cultured cells.," Proc Natl Acad Sci U S A, vol. 68, pp. 2127–2130, Sep 1971.

[24] K. K. Sanford, G. L. Hobbs, and W. R. Earle, "The tumor-producing capacity of strain l mouse cells after 10 years in vitro.," Cancer Res, vol. 16, pp. 162–166, Feb 1956.

[25] G. J. Todaro, H. Grenn, and M.D., "Quantitative studies of the growth of mouse embryo cells in culture and their development into established lines.," The Journal of Cell Biology, vol. 17, pp. 299–313, 1963.

[26] R. Pethig and G. H. Markx, "Applications of dielectrophoresis in biotechnology.," Trends Biotechnol, vol. 15, pp. 426–432, Oct 1997.

[27] M. S. Jaeger, T. Mueller, and T. Schnelle, "Thermometry in dielectrophoresis chips for contact-free cell handling," J. Phys. D: Appl. Phys., vol. 40, pp. 95–105, 2007.

[28] P. Somasundaran, Encyclopedia of Surface and Colloid Science. CRC Press Inc, 2006.

[29] R. Glaser, Biophysics. Springer, 2001.

[30] V. L. Sukhorukov, H. Mussauer, and U. Zimmermann, "The effect of electrical deformation forces on the electropermeabilization of erythrocyte membranes in low- and high-conductivity media.," J Membr Biol, vol. 163, pp. 235–245, Jun 1998.

[31] T. B. Jones, Electromechanics of Particles. Cambridge University Press, 1995.

[32] J. Gimsa and D. Wachner, "A polarization model overcoming the geometric restrictions of the laplace solution for spheroidal cells: obtaining new equations for field-induced forces and transmembrane potential.," Biophys J, vol. 77, pp. 1316–1326, Sep 1999.

[33] F. Thom and H. Gollek, "Calculation of mechanical properties of human

red cells based on electrically induced deformation experiments," Journal of Electrostatics, vol. 64, pp. 53–61, 2006.

[34] U. Zimmermann, U. Friedrich, H. Mussauer, P. Gessner, K. Hamel, and V. Sukhorukov, "Electromanipulation of mammalian cells: fundamentals and application," Plasma Science, IEEE Transactions on, vol. 28, no. 1, pp. 72–82, 2000.

[35] B. Alberts, A. Johnson, J. Lewis, M. Raff, K. Roberts, and P. Walter, Molecular biology of the cell. Garland Science, 2002.

[36] D. Bray, Cell Movements. Garland, 1992.

[37] P. A. Janmey, U. Euteneuer, P. Traub, and M. Schliwa, "Viscoelastic properties of vimentin compared with other filamentous biopolymer networks.," J Cell Biol, vol. 113, pp. 155–160, Apr 1991.

[38] Y. C. Fung, Biomechanics. Mechanical properties of living tissue. Springer - Verlag, 1993.

[39] J. P. Butler and S. M. Kelly, "A model for cytoplasmic rheology consistent with magnetic twisting cytometry.," Biorheology, vol. 35, no. 3, pp. 193–209, 1998.

[40] S.-M. Ahn, S.-J. Jeong, Y.-S. Kim, Y. Sohn, and A. Moon, "Retroviral delivery of timp-2 inhibits h-ras-induced migration and invasion in mcf10a human breast epithelial cells.," Cancer Lett, vol. 207, pp. 49–57, Apr 2004.

[41] E.-S. Kim, M.-S. Kim, and A. Moon, "Transforming growth factor (tgf)-beta in conjunction with h-ras activation promotes malignant progression of mcf10a breast epithelial cells.," Cytokine, vol. 29, pp. 84–91, Jan 2005.

[42] S. S. Martin and P. Leder, "Human mcf10a mammary epithelial cells undergo apoptosis following actin depolymerization that is independent of attachment and rescued by bcl-2.," Mol Cell Biol, vol. 21, pp. 6529–6536, Oct 2001.

[43] B. C. Spink, R. W. Cole, B. H. Katz, J. F. Gierthy, L. M. Bradley, and D. C. Spink, "Inhibition of mcf-7 breast cancer cell proliferation by mcf-10a breast epithelial cells in coculture.," Cell Biol Int, vol. 30, pp. 227–238, Mar 2006.

[44] K. Ciftci, J. Su, and P. B. Trovitch, "Growth factors and chemotherapeutic modulation of breast cancer cells.," J Pharm Pharmacol, vol. 55, pp. 1135–1141, Aug 2003.

[45] H. Zientek-Targosz, D. Kunnev, L. Hawthorn, M. Venkov, S.-I. Matsui, R. T. Cheney, and Y. Ionov, "Transformation of mcf-10a cells by random mutagenesis with frameshift mutagen icr191: a model for identifying candidate breast-tumor suppressors.," Mol Cancer, vol. 7, p. 51, 2008.

[46] S. W. Park and R. A. Scapery, "Methods of interconversion between linear viscoelastic material functions. part i - a numerical method based on prony series," Int. J. Solids Struct., vol. 36, pp. 1653–1675, 1999.

[47] F. Wottawah, S. Schinkinger, B. L. R, Ananthakrishnan, M. Romeyke, J. Guck, and J. Kaes, "Optical rheology of biological cells," Physical review letters, vol. 94(9), pp. 98–103, 2005.

[48] C. Polk and E. Postow, eds., Handbook of Biological Effects of Electromagnetic Fields. CRC, 1986.

[49] T. Schnelle, T. Mueller, and G. Fuhr, "Dielectric single particle spectroscopy for measurement of dispersion.," Med Biol Eng Comput, vol. 37, pp. 264–271, Mar 1999.

[50] M. Castellarnau, A. Errachid, C. Madrid, A. Juárez, and J. Samitier, "Dielectrophoresis as a tool to characterize and differentiate isogenic mutants of escherichia coli.," Biophys J, vol. 91, pp. 3937–3945, Nov 2006.

[51] K. Ratanachoo, P. R. C. Gascoyne, and M. Ruchirawat, "Detection of cellular responses to toxicants by dielectrophoresis.," Biochim Biophys Acta, vol. 1564, pp. 449–458, Aug 2002.

[52] L. M. Broche, N. Bhadal, M. P. Lewis, S. Porter, M. P. Hughes, and F. H. Labeed, "Early detection of oral cancer - is dielectrophoresis the answer?," Oral Oncol, vol. 43, pp. 199–203, Feb 2007.

[53] J. An, J. Lee, S. H. Lee, J. Park, and B. Kim, "Separation of malignant human breast cancer epithelial cells from healthy epithelial cells using an advanced dielectrophoresis-activated cell sorter (dacs).," Anal Bioanal Chem, vol. 394, pp. 801–809, Jun 2009.

[54] J. L. Sebastián, S. M. S. Martín, M. Sancho, and J. M. Miranda, "Modelling the internal field distribution in human erythrocytes exposed to mw radiation.," Bioelectrochemistry, vol. 64, pp. 39–45, Aug 2004.

[55] N. Wang, "Mechanical interactions among cytoskeletal filaments.," Hypertension, vol. 32, pp. 162–165, Jul 1998.

[56] C. Rotsch and Radmacher, "Drug-induced changes of cytoskeletal structure and mechanics in fibroblasts: an atomic force microscopy study.," Biophys J, vol. 78, pp. 520–535, Jan 2000.

[57] E. D. Salmon, M. McKeel, and T. Hays, "Rapid rate of tubulin dissociation from microtubules in the mitotic spindle in vivo measured by blocking polymerization with colchicine.," J Cell Biol, vol. 99, pp. 1066–1075, Sep 1984.

[58] I. Spector, N. R. Shochet, Y. Kashman, and A. Groweiss, "Latrunculins: novel marine toxins that disrupt microfilament organization in cultured cells.," Science, vol. 219, pp. 493–495, Feb 1983.

[59] B. Ludin and A. Matus, "Gfp illuminates the cytoskeleton.," Trends Cell Biol, vol. 8, pp. 72–77, Feb 1998.

[60] H. Engelhardt and E. Sackmann, "On the measurement of shear elastic moduli and viscosities of erythrocyte plasma membranes by transient deforma-

tion in high frequency electric fields.," Biophys J, vol. 54, pp. 495–508, Sep 1988.

[61] M. Kirschbaum, M. S. Jaeger, T. Schenkel, T. Breinig, A. Meyerhans, and C. Duschl, "T cell activation on a single-cell level in dielectrophoresis-based microfluidic devices.," J Chromatogr A, vol. 1202, pp. 83–89, Aug 2008.

List of symbols

AC	alternanting current
C_m	membrane electric capacitance
d	distance
DC	direct current
DEP	dielectrophoresis
E	Electric field
F	Force
f	frequency
$F_{i,i=1,2,3}$	force plateaus
$f_{i,i=1,2}$	crossover frequency
F_DEP	dielectrophoretic force
f_{ex}	experimental frequency
$\mathbf{F}_F$	drag force

G_e	elastic modulus
GFP	green fluorescent protein
G_m	membrane electric conductivity
G_p	yield stress
j	imaginary unit
k	thermal and geometrical factor
$K(\omega)$	Clausius-Mossotti factor
l	length
m	dipole moment
q	electric charge
Q	heat conduction
r	cell radius
R_{ex}	external medium resistance
Re[f_{cm}]	real part of Clausius-Mossotti factor
R_{in}	internal resistance
R_m	membrane resistor
S	surface
T	temperature
T_0	ambient temperature
v	cell velocity
v_∞	terminal velocity for the steady state
V_{rms}, V	voltage amplitude

α	dispersion region
β	dispersion region
Δ	delta operator
γ	dispersion region
ε	permittivity
ε	cell deformation
ε_{in}	internal permittivity
ε_o	permittivity of free space
η	viscosity
λ	thermal conductivity
η_e	viscosity of elastic element
η_p	viscosity of plastic element

ρ	mass density
ϱ	deformation of viscoelastic element
$\sigma(\omega)$	electric conductivity
σ	stress
σ_e	stress for elastic element
σ_{ex}	external electric conductivity
σ_{in}	internal electric conductivity
σ_m	electric conductivity of the medium
σ_p	electric conductivity of the particle
σ_v	stress for plastic element
τ	time constant
τ_a	time of acceleration
φ	deformation of viscoplastic element
ω	angular frequency
∇	nabla operator

List of Figures

List of publications

Journal article

I. Guido, M. S Jäger, C. Duschl. Dielectrophoretic stretching of cells allows characterization of their mechanical properties. Journal of Biomechanics, (submitted).

Talks

Cell deformability by dielectrophoretic fields. Medical Physics and Biomedical Engineering World Congress 2009, 11.09.2009

Electric deformability as a new cellular marker, Workshop: Bioanalytik-Nachwuchstreffen, Luckenwalde, 19.11.2007

Posters

I. Guido, M. Jäger, C. Duschl. Dielectrophoretic stretching for single cell identification, 23th Meeting Medical Engineering, Biomedical Engineering for therapeutic Oncology, Berlin, 04.06.2009

I. Guido, M. Jäger, C. Duschl. Dielectrophoretic stretching for single cell identification, FEBS Workshop Mechanics and Dynamics of the Cytoskeleton, Potsdam, 22.-26.06.2008.

I. Guido, M. Jäger, C. Duschl. Dielectrophoretic stretching for single cell identification, Biosystems conference, Berlin, 28.06.2006